6-1-1997

Modeling the effect of ink spread and ink penetration on tone reproduction

Michael Alber

MODELING THE EFFECT OF INK SPREAD AND INK PENETRATION ON TONE REPRODUCTION

by

MICHAEL L. ALBER

B.S. Rochester Institute of Technology

(1991)

A thesis submitted in partial fulfillment of the
requirements for the degree of Master of Science
in the Chester F. Carlson Center for Imaging Science
of the College of Science
Rochester Institute of Technology

June 1997

Signature of Author _____

Accepted by H. E. Rhody 6/25/97

Coordinator, M.S. Degree Program Date

CHESTER F. CARLSON
CENTER FOR IMAGING SCIENCE
COLLEGE OF SCIENCE
ROCHESTER INSTITUTE OF TECHNOLOGY
ROCHESTER, NEW YORK

CERTIFICATE OF APPROVAL

M.S. DEGREE THESIS

The M.S. Degree Thesis of Michael L. Alber
has been examined and approved by the
thesis committee as satisfactory for the
thesis requirement for the
Master of Science degree

Dr. Jonathon S. Arney

Dr. Roy S. Berns

Dr. Ethan Montag

June 25, 1997
Date

CHESTER F. CARLSON
CENTER FOR IMAGING SCIENCE
COLLEGE OF SCIENCE
ROCHESTER INSTITUTE OF TECHNOLOGY
ROCHESTER, NEW YORK

THESIS RELEASE PERMISSION

Title of Thesis: *Modeling the Effect of Ink Spread and Ink Penetration on Tone Reproduction*

I, Michael L. Alber, hereby grant permission to the Wallace Memorial Library of R.I.T. to reproduce my thesis in whole or in part. Any reproduction will not be for commercial use or profit.

Signature:_____ Date: 6/26/97

Modeling the Effect of
Ink Spread and Ink Penetration
on Tone Reproduction

by

Michael L. Alber

submitted to the
Chester F. Carlson
Center for Imaging Science
College of Science
in partial fulfillment of the requirements
for the Master of Science Degree
at the Rochester Institute of Technology

ABSTRACT

In ink jet printing when ink is printed on top of the paper, two effects occur that have an effect on the dot that is printed. One effect is that the ink spreads out laterally and the other is that the ink penetrates into the paper. A tone reproduction model was developed that mathematically modeled the effects ink spread and ink penetration have on tone reproduction. Since the optical behavior of ink penetration is very complex, the model only included characteristics that were expected to be significant. This model was built from the foundation of another tone reproduction model which mathematically modeled the optical effect of halftone patterns as a probability. The model was tested using test samples consisting of gray scales produced by thermal ink jet. These samples were produced by varying certain conditions that are thought to affect ink penetration and ink spread and simulate other ink jet environments such as different inks, different papers, and different printers. Microdensitometry equipment was used to obtain data from the samples and the model was analyzed on how well it fit the data.

ACKNOWLEDGEMENTS

I'd like to thank...

My advisor, Dr. Arney, for being so helpful and patient.

DuPont, for their help.

My good friend, Nicole Smith, who really helped me through this. Thanks for the support.

My lab partners, Dave Stewart, Miako Katsube, Tuo Wu, and Hung Tran,who kept me company in the lab and were fun to be around.

My parents, Jan and Rich, and my brother, Dave, for being so supportive.

TABLE OF CONTENTS

TABLE OF CONTENTS
(continued)

LIST OF FIGURES

LIST OF FIGURES
(continued)

LIST OF FIGURES
(continued)

LIST OF FIGURES
(continued)

LIST OF TABLES

GLOSSARY OF TERMS

Light absorption strength or light absorption efficiency: Term used to describe how well the colorant particles are at absorbing photons.

Single color print: Term used for a halftone pattern that consisted of halftone dots of one color.

Two color overprint: Term used for a halftone pattern that consisted of halftone dots of two colors.

Image microstructure data: Term used for data collected from a halftone pattern the consisted of the reflectance of the paper between the dots, the ink reflectance, the overall reflectance of the halftone pattern, and the dot area fraction.

Microdensitometry equipment: Term used for describing the equipment used for measuring the image microstructure data. The equipment consisted of a microscope with a CCD camera attached to it which was connected to a computer.

Arney-Katsube Probability Model: A tone reproduction model that algebraically models image microstructure data by modeling the scattering nature of light in paper as a probability.

Modified Probability Model: A tone reproduction model developed from the Arney-Katsube Probability Model that considered ink penetration and ink spread.

Printing conditions: Term used for describing the conditions a halftone pattern would be printed at. These conditions would consist of the type of paper, type of ink, type of printer, and heat applied and not applied to the paper.

Line scan: A one dimensional scan of optical density vs. distance across halftone dots.

GLOSSARY OF PARAMETERS

(parmeters are used in the Modified Probability Model in section 3.9)

F: Dot area fraction.

F_o: Dot area fraction command to the printer.

R: Average reflectance of halftone pattern.

R_i: Average ink reflectance of halftone dot.

R_{i1}: Reflectance component of halftone dot that scatters light for light incident from beneath the dot.

R_{i2}: Reflectance component of halftone dot that scatters light for light incident on top of the dot.

R_p: Average reflectance of the paper between the dots.

R_g: Intrinsic reflectance of the paper substrate at $F = 0$.

T_i: Transmittance of the halftone dot.

S: Kubelka-Munk's scattering coefficient (units in cm^{-1}).

K: Kubelka-Munk's absorption coefficient (units in cm^{-1}).

x: Height of dot (units in cm).

a, b: Kubelka-Munk parameters.

Sx: The product of S and x which correlates with light scattering in ink (correlates with ink penetration).

w: Light spread in paper (correlates with optical dot gain).

ε: Beer-Lambert's extinction coefficient (correlates with absorption strength of ink).

GLOSSARY OF PARAMETERS
(continued)

(parmeters are used in the Modified Probability Model in section 3.9)

P_p:Probability light entering between the dots emerges beneath the dots.

P_i: Probability light entering the paper after transmitting through the dots emerges from the paper beneath the dots.

P_{po}: Probability light entering between the dots emerges beneath the dots for a dot that does not scatter light.

C: Concentration of colorant (units in g/m^3).

C_c: Ink coverage (units in g/m^2).

C_o: Maximum ink coverage (units in g/m^2).

A: Empirical constant dependent on halftone geometry utilized in equation for the w parameter.

k_p: Mean lateral scattering distance scattering distance of photons in paper (units in mm).

f: Screen frequency of halftone pattern.

1. Introduction

The ink jet printing process is considered to be a binary process in producing halftone images since a drop of ink is either laid down or not. The dots are of only one shade and the tone of an area is controlled by the amount of area the dots cover.

Ink spread and ink penetration are two effects that occur in the paper-ink interaction of ink jet printing and are known to affect the characteristics of a halftone dot. As ink spreads, the halftone dot increases in size and becomes less dark. As ink penetrates into the paper, the paper causes the light entering into the ink to scatter. A model was designed that has been capable of describing the effect ink spread and ink penetration have on tone reproduction. It was developed from a tone reproduction model which is known as the Arney-Katsube Probability Model.[1,2] The Probability Model was modified by including empirically derived equations for parameters in the model so that the parameters simulated ink spread and ink penetration.

To test the model, samples were generated by thermal ink jet printing. The samples were produced under different printing conditions (different inks, different papers, heat applied and not applied to the paper, and different printers) that affect ink spread and ink penetration and that were to represent other ink jet system environments. Microdensitometry equipment was used to measure data from these samples. The model was evaluated on how well the measured data fit the model and how well the model's

parameters were able to explain the effects the printing conditions have on the inherent properties of the ink.

2. Objective

The intent of this research was to mathematically model the effects ink spread and ink penetration have on tone reproduction based on physical and optical properties of the system. This was performed by mathematically adjusting parameters in the Probability Model that were affected by ink spread and ink penetration to have them simulate the effects these two mechanisms have on them. This model was tested by producing several ink jet gray scale test samples with different conditions that were thought to affect ink penetration and ink spread and to simulate other ink jet environments.

3. Background

Since the investigation of this research is focused on ink spread and ink penetration of ink jet printers, it would be helpful to understand some of the basic technology of ink jet printers. A review of the basic principles of ink jet printer technology will be introduced. Next, the physics of the optics and basic makeup of paper and ink will be discussed. Following that a review of the principles of halftone dot gain and the histogram characteristics of halftone dots will be presented. Since the research is involved with designing a tone reproduction model, some older tone reproduction models will be shown that are also helpful in describing some fundamental principles of halftone patterns. The Arney-Katsube Probability Model will be introduced which is the base for the model developed for this research. Lastly the Modified Probability Model, which is the model developed for this research, will be introduced.

3.1 Ink Jet Printers

Ink jet printers attempt to reproduce the appearance of a single dot on a computer monitor (known as a pixel) into its corresponding tone and color on the printing material by use of halftoning techniques. The luminance of the pixel is calibrated into 255 equal divisions and each luminance level is represented by an electronic computer parameter called a gray level, G. Gray levels range from 0 (lowest light level, darkest) to 255 (highest light level, lightest). Ink jet printers simulate the light intensity on hardcopy by the number of drops of ink placed inside a certain area. The more drops of ink placed inside an area, the darker the region. When the computer instructs the printer to print at a certain gray level G, the printer will lay down a certain number of drops within a certain area to represent the luminance of the pixel. The percent area the drops of ink actually occupy is called the dot area fraction, F

This actual dot area fraction, F, usually does not coincide with the dot area fraction the ink jet printer tries to cover, F_o (ideal dot area fraction). An example would be if F_o was 25%. Digitally, it would be easier to produce F equal to 25% if the dots were square in shape.

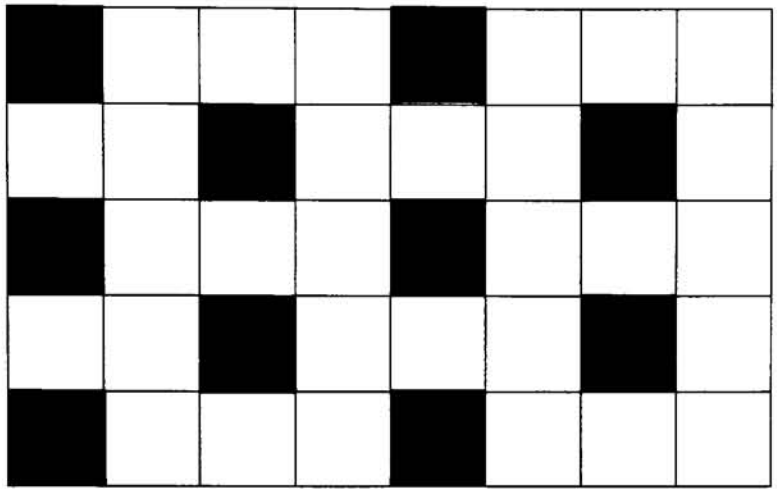

Figure 3.1.1: If ink jet dots were square in shape, digitally it would be easier to represent F_o as 25% (*F=10/40*).

Since ink drops produce circular dots, the dots may be smaller than the area of a square dot which would give the amount of area covered to be less than 25%. (Note: This is only displayed for a hypothetical purpose since in reality the physical size of ink jet dots are larger than ideal ink jet dots)

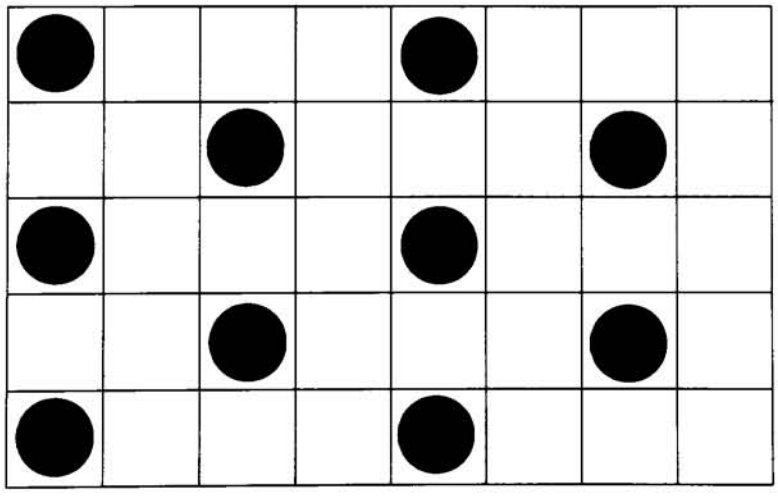

Figure 3.1.2: Ink jet dots are circular in shape and can be smaller than a square dot. The area covered would be less than 25%.

The dots can also be larger than square dots covering more than 25% of the area.

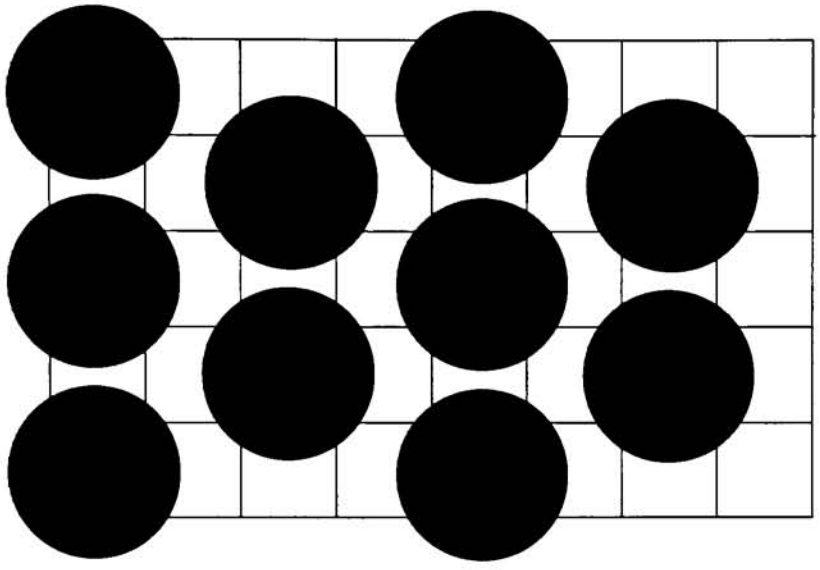

Figure 3.1.3: Ink jet dots can also be larger than a square dot covering more than 25% of the area.

Ink jet dots can be misplaced due to misalignment of the ink cartridges. It is unknown if F is greater than or less than 25% as shown in figure 3.1.4.

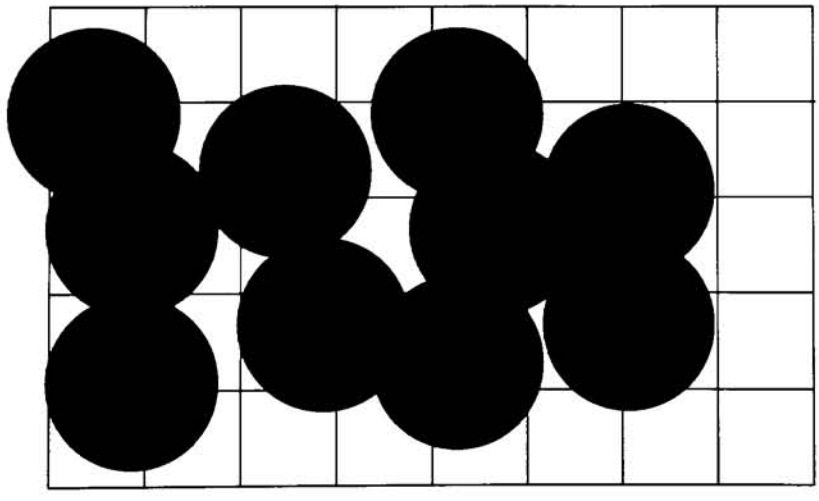

Figure 3.1.4: Ink jet dots can be misplaced due to the misalignment of ink cartridges. It is unknown if F is larger or smaller than 25%.

There are various ways ink jet drops are produced and laid on paper depending on the type of ink jet printer utilized. Ink jet printers are broken down into two categories: continuous jet and drop-on-demand jet. Continuous ink jet printing involves the displacement of an ionized stream of ink drops through a voltage controlled electric field. In drop-on-demand ink jet printing, the ink drops are released from the nozzles when instructed.

Drop-on-demand ink jet printers are classified by the driver type: piezoelectric and thermal or bubble jet. Currently, the market place is dominated by thermal ink jet printers. 90% to 95% of the market share is thermal ink jet printers.[3]

Piezoelectric ink jet printers produce ink drops by inducing a voltage on a polarized ceramic element which deforms and creates an acoustic wave in the fluid cavity. In thermal ink jet printers, ink drops are created by applying voltage on a resistive element which heats the ink in the fluid cavity and creates a bubble. When the bubble bursts, the ink drop is propelled out of the nozzle.

Since the ink in thermal ink jet printer must be heated enough to create a bubble, the ink needs to be composed of a volatile component that is capable of vaporizing and is formulated so when the ink is heated no residues are produced to clog the nozzles. Thermal ink jet ink is typically water-based. Piezoelectric ink jet printers, due to their nature, are not as limited to the type of ink used and can use almost any type of fluid.[3]

The quality of thermal ink jet images is dependent on the interaction between the ink and paper and is greatly influence by the type of paper used. Ink jet images are composed of drops of ink. When a drop of ink is delivered to the paper, there is a delay in time before the capillary action of the paper absorbs the ink. This is dependent on the hydrophobicity of the paper. After the delay, the water in the ink begins to evaporate and diffusion and sorption occurs which wet the paper fibers. After wetting of the paper occurs, capillary action takes place in the paper until the ink is penetrated and dried. During this stage, ink can spread laterally and can flow down into the paper. Thus, the three main mechanisms in ink-paper interaction are wetting, penetration, and spreading.[4] What will be analyzed in this research are the effects ink penetration and ink spread have on tone reproduction.

3.2 Paper and Ink

Paper consists of a mat of vegetable fibers which are essentially transparent. Paper appears white due to the scattering and reflecting effect caused by the fibers. When light strikes paper, the light is either reflected (known as specular reflection or gloss), transmitted, scattered, or absorbed.[5]

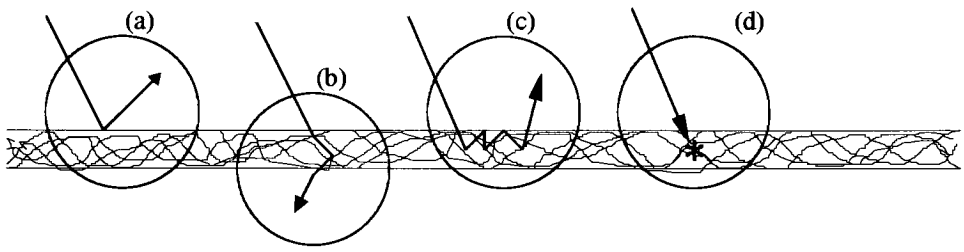

Figure 3.2.1: Four effects that occur to light when it strikes uncoated paper: (a) reflection (known as specular reflection or gloss), (b) transmission, (c) scattering, and (d) absorption.

Paper is classified as being either coated and uncoated. For coated paper, a layer of fine particles is laid on top of the paper to enhance its appearance and its printability. This layer scatters light more than the paper as shown in figure 3.2.2. Uncoated paper does not have this layer.

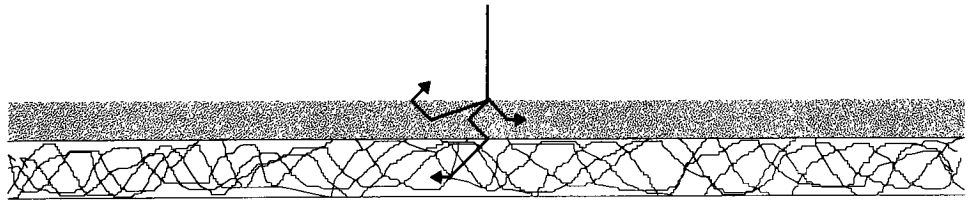

Figure 3.2.2: In coated paper, the coated layer scatters more light than the paper layer.

Paper is also manufactured from man-made materials such as polymers. This type of paper is known as synthetic paper and does not contain vegetable fibers.

Since paper scatters light, the lateral spread of light as it enters into paper can be modeled as a point spread function, PSF, or a modulation transfer function, MTF (Fourier equivalent to the PSF). From a past study, equations for these functions can be modeled using the following empirically derived equations.[1,6]

$$PSF(x) = \frac{1}{k_p} K_0\left(\frac{2\pi x}{k_p}\right) \tag{3.2.1}$$

$$MTF(\omega) = \frac{1}{1 + \left(k_p \omega\right)^2} \tag{3.2.2}$$

where, x: distance from the point light enters paper (in units of mm)

ω: spatial frequency in the Fourier domain (in units of mm^{-1})

k_p: constant proportional to mean lateral distance light travels in paper (in units of mm)

K_o: Bessel function of the third kind[24]

Ink consists of two main components: the colorant and the vehicle. The vehicle is a liquid which is to suspend or dissolve the colorant and to dry and affix the colorant to the printing surface.[7] Colorants are classified as dyes or pigments. Dyes are soluble organic colorants and pigments are insoluble organic or inorganic colorants. Dyes exist

in a monomolecular state and pigments consist of particles (0.1 to 1.0 microns) with a large number of molecules.

The main factors that affect the transmittance for both dyes and pigments are the concentration of the colorant, the thickness of the ink film, and the chemical composition.[8] Beer-Lambert theory mathematically correlates the optical transmittance of the ink with the thickness of the ink film and the concentration of the colorant with the following equation.

$$T_i = 10^{-\varepsilon C x} \tag{3.2.3}$$

where, ε: extinction coefficient (in units of m^2/g)

C: concentration of colorant (in units of g/m^3)

x: thickness of the ink film (in units of meters)

Dyes are more efficient at absorbing photons than pigments due to their monomolecular state since each molecule absorbs a photon. For pigments, the molecules on the surface absorb photons so pigments are tinctorially weaker and are generally of lower chroma.[9]

Most printing inks are transparent.[10] What makes inks transparent is the amount of scattering of the light that occurs. Since dyes are monomolecular, there are no discrete particles and therefore, no scattering of light occurs. Thus, dye-based inks are transparent.

Pigment-based inks do scatter light and are considered to be more opaque. The scattering of light is mainly caused by the size of the pigment particles and the difference in the index of refraction between the pigment and the vehicle. A pigment particle size is close to the wavelength of visible light (0.4 to 0.7 microns) and hence, white light is scattered. The greater the difference in the index of refraction between the pigment and the vehicle, the more scattering of white light will occur. Other factors that affect the scattering of light are particle shape, aggregation, and the wavelength of the light.[8]

3.3 Dot Gain

In the halftoning process, when a dot is laid on paper, the printed dot size is never the same as the intended dot size. This deviation from intended size is known as dot gain. A dot size is affected both physically and optically. Thus, dot gain is categorized into two effects: physical dot gain and optical dot gain. The first effect, "physical dot gain", is when the ink does not stay within its boundaries but spreads out. An example is when an ink jet drop laterally diffuses when it strikes the paper or when ink spreads laterally as it transfers from a lithographic plate. The second effect, "optical dot gain" or more commonly known as the "Yule-Nielson effect", is due to the scattering nature of the paper. Figure 3.3.1 illustrates the Yule-Nielson effect.

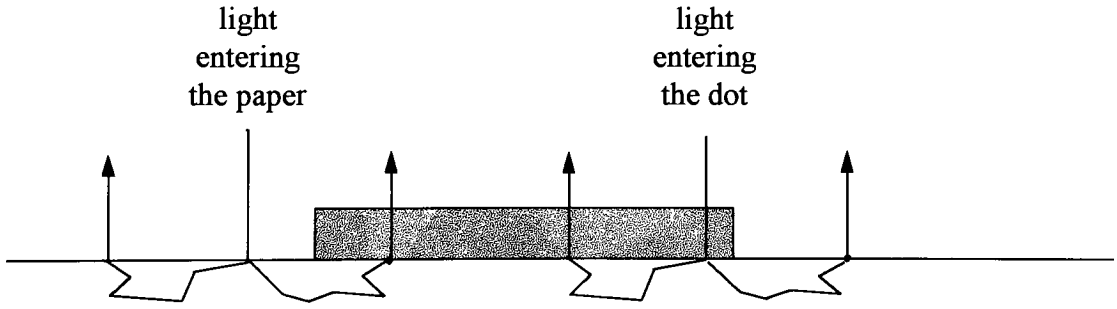

Figure 3.3.1: Optical dot gain or more commonly known as the "Yule-Nielson effect."

As shown, part of the light entering the paper portion is absorbed by the dot. Also, part of the light which enters the dot exits through the paper which also affects optical dot gain. This portion of light is small compared to the light entering the paper

and exiting through the dot. The dot will be the same physical size but will appear to have a halo around it. This is illustrated in figure 3.3.2.[11]

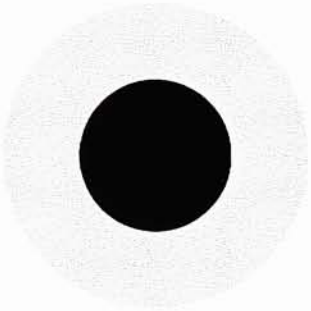

Figure 3.3.2: Due to the scattering nature of light in paper, a halftone dot will appear to have a halo around it. This is due to the dot absorbing light that is incident on the paper but enters into the dot. This results in optical dot gain.

3.4 Histogram Characteristics of Halftone Dot Patterns

The histogram of an ideal halftone pattern consists of two spikes as displayed in figures 3.4.1 (a) and (b). The paper reflectance (R_p) and ink reflectance (R_i) would be uniform and of one value. In figure 3.4.1 (a) the ink reflectance is 0.2 and the paper reflectance is 0.9 at a dot area fraction (F) of 25%. As the dot area fraction increases for the ideal halftone pattern, the spikes would stay in place except change in height as shown in figure 3.4.1 (b) for F equal to 0.9.

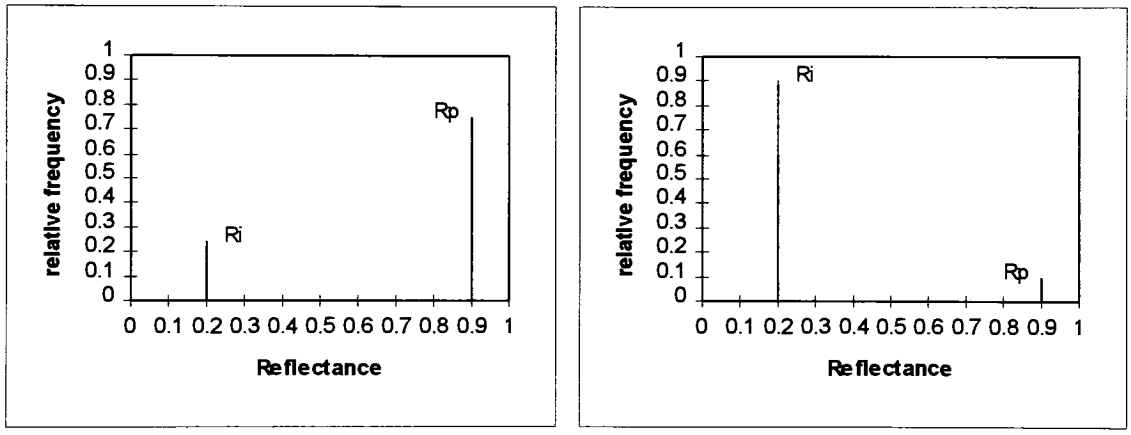

(a) (b)

Figure 3.4.1: Histograms of an ideal halftone pattern with (a) having a dot area fraction of 25% and (b) having a dot area fraction of 90%.

Figure 3.4.2 is a histogram of a real halftone dot pattern. Notice how R_i and R_p are not spikes. Also note the transition region of which is the region on the histogram that indicates the reflectances that are on or near the edge of the dot. The transition

reflectance (R_t) is the reflectance located on the transition point which is the point on the edge of the dot where the rate of change of the reflectance, dR/dx, is maximum. On the histogram, the transition reflectance is indicated by the lowest part of the valley between the two peaks. The dot area fraction is calculated from the histogram by calculating the area (A_1) of the histogram up to the transition point divided by the area of the histogram ($A_1 + A_2$).

$$F = \frac{A_1}{A_1 + A_2} \tag{3.4.1}$$

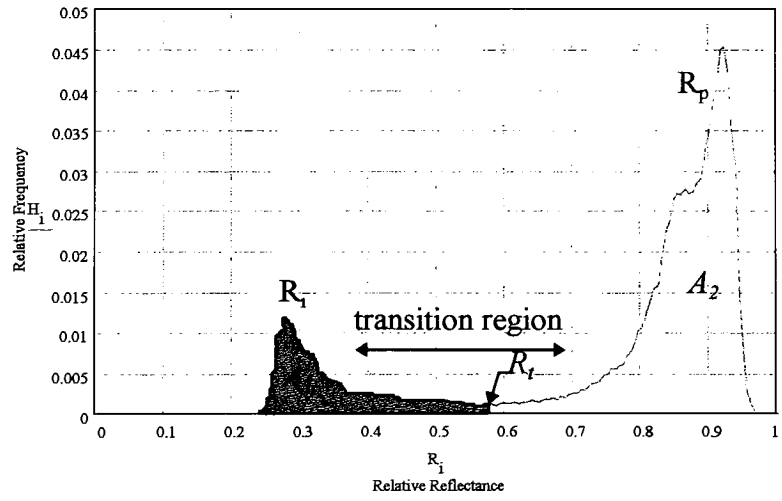

Figure 3.4.2: Histogram of a real halftone pattern. The transition region is the region of reflectances that are on or near the edge of the dot.

Two main effects cause R_i and R_p to not be spikes. One effect is the light scattering properties of the paper (optical dot gain) and the other effect is the

nonuniformity of ink and paper reflectances. Figure 3.4.3 displays a hypothetical histogram that illustrates the affect of these two effects. The nonuniformity of the R_i and R_p causes the spikes to be gausian in shape since some reflectances would be greater than or less than the mean reflectance as shown in figure 3.4.3 (a). The scattering nature of the paper causes the edge of the dot to become lighter causing the reflectances on the edge to increase in value as shown in figure 3.4.3 (b). Also, the scattering nature of the paper causes the paper to become darker near the edge of the dot causing the reflectances to decrease in value as shown in figure 3.4.3 (b).

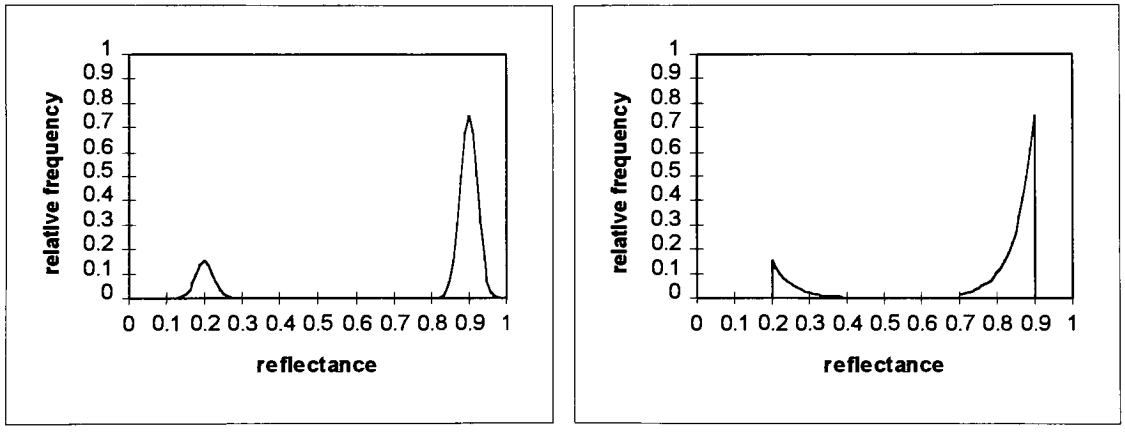

(a) (b)

Figure 3.4.3: Hypothetical histograms demonstrating the effect of (a) the nonuniformity of ink reflectances and paper reflectances and (b) the effect of the light scattering nature of paper.

One last property that occurs in histograms is that as the dot area fraction increases the R_i peak and R_p peak shift to the left. This is displayed in figure 3.4.4. This is also due to the light scattering nature of the paper. The dots absorb light that is

incident on top of them and also light that is scattered by the paper underneath them that affect the average reflectance of the R_i and R_p.

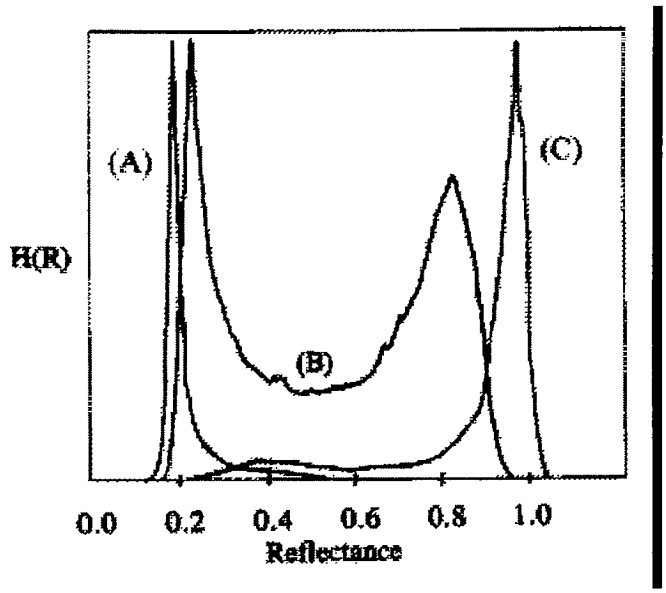

Figure 3.4.4: The above histograms demonstrate that as the dot area fraction increases the histograms' peaks shift to the left. The dot area fractions are (a) F=0.90, (b) F=0.50, and (c) F=0.05.

Figure 3.4.5 gives a better demonstration of why the histograms shift. When F is near 0.0, the dots are very small and most of the light from the dot is from light incident on the paper. The reflectance of the paper is the reflectance of the bulk paper, R_g, and the reflectance of the ink is $R_g T_i$. The R_p peak of the histogram is centered on R_g and the R_i peak is centered on $R_g T_i$ at F equal to 0.0. As F increases and approaches 1.0, the ink covers most of the paper and most of the light from the paper is from light incident on

the ink. The reflectance of the ink is $R_g T_i^2$ and the reflectance of the paper is $R_g T_i$. The R_p peak is centered on $R_g T_i$ and the R_i peak is centered on $R_g T_i^2$ at F equal to 1.0. Hence, in theory as F goes from 0.0 to 1.0, R_i goes from $R_g T_i$ to $R_g T_i^2$ and R_p goes from R_g to $R_g T_i$.[13]

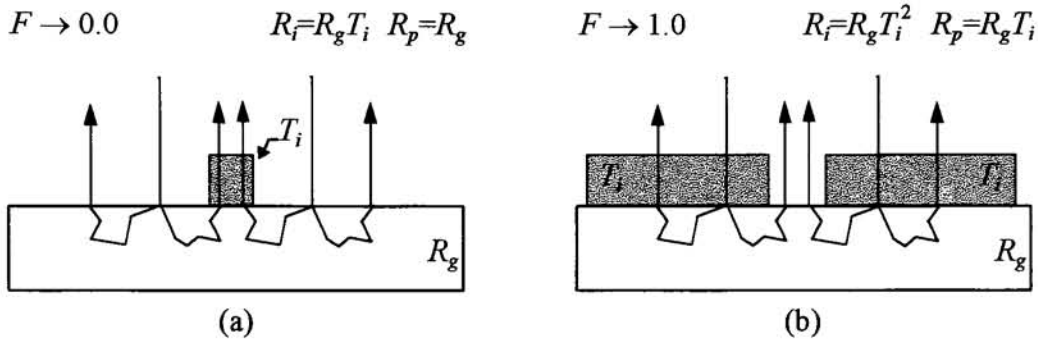

Figure 3.4.5: In theory as F goes from 0.0 to 1.0, R_i goes from $R_g T_i$ to $R_g T_i^2$ and R_p goes from R_g to $R_g T_i$. This affects the histogram of a halftone pattern by causing the R_i peak and R_p peak to shift to the left as F increases.

3.5 Ink Spread and Ink Penetration

When ink spreads, the ink film becomes thinner and the dot size becomes larger as illustrated in figure 3.5.1. As was mentioned in section 3.2, one of the main factors that affect the transmittance of colorants is the thickness of the ink film of which is noted in Beer-Lambert theory. Other factors that affect the darkness of the dot are first surface reflectance (light that is scattered on the dot's surface before being absorbed or transmitted through), scattering of light within the ink, and the amount of light that is absorbed by the paper. These factors are generally considered to be minor compared to the thickness of the ink film.[12] Hence, ink spread causes a dot to be less dark and to be larger in size.

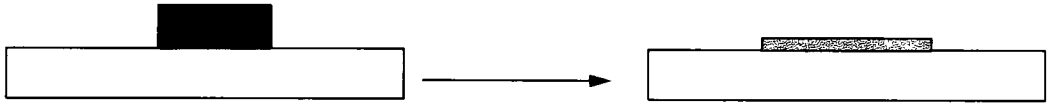

Figure 3.5.1: Ink Spread affects a halftone dot by increasing its size and decreasing its thickness.

As ink penetrates into the paper, the paper causes the light that enters into the ink to scatter. Hence, the effect ink penetration has on a halftone dot is that it causes the light within the dot to scatter. In the printing industry, it is desirable to have the ink to lay on top of the paper. Paper that does not allow ink to penetrate is said to have "good hold-out."

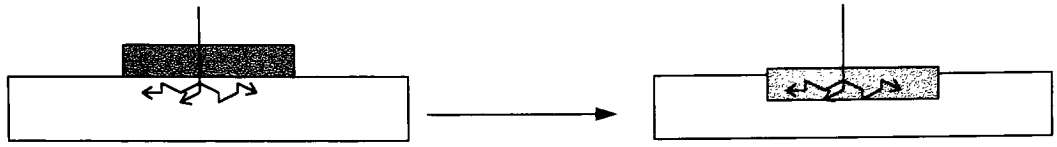

Figure 3.5.2: As ink penetrates into the paper, the light entering the dot will scatter more due to the scattering nature of the paper.

3.6 Murray-Davies Model

The first tone reproduction model developed was the "Murray-Davies model" which stated that the reflectance of the halftone pattern, R, was the average spatial reflectance of the paper reflectance, R_p, and the ink reflectance, R_i. The following is the equation for the Murray-Davies model.

$$R = FR_i + (1 - F)R_P \tag{3.6.1}$$

F is the fractional area the ink covers. R_i and R_p are considered to be constants. Note, that R is in linear relationship to F.

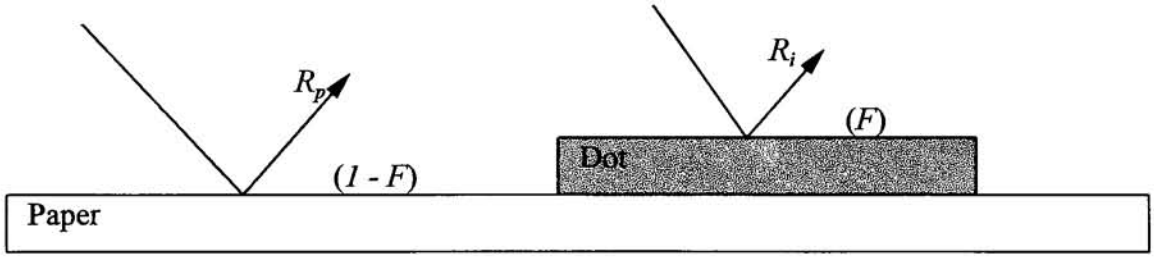

Figure 3.6.1: A visual illustration portraying the Murray-Davies model.

The Murray-Davies model can be essentially seen as a law of conservation of energy (as in photon energy). Photon flux from the surface add linearly. Reflectances are linearly related to photon flux and thus, reflectances are expected to add linearly.[13]

Yule and Nielson observed that R was linear to F for substrates that do not scatter light (transparencies, silver mirror surface, etc.). For substrates that do scatter light (paper, opal glass, etc), R was no longer linear to F due to optical dot gain. The dot

actually absorbed more light since it affected the photon flux in the surrounding areas. As was mentioned in section 3.3, this can be visually viewed as the halo that surrounds the dot. Thus, the halftone pattern appears darker than predicted by the Murray-Davies model.

Although the Murray-Davies model recognizes that R_p and R_i are constant, studies have shown for scattering substrates that R_p and R_i are themselves functions of F [13] Thus, the Murray-Davies model fails if R_p and R_i are taken as constants. As mentioned above, the Murray-Davies equation must be correct if it is looked at as the law of conservation of energy. However, eq. 3.6.1 can be empirically modified to match the observed effect of optical dot gain if R_p and R_i are not taken as constants.

3.7 Yule-Nielson Model

The "Yule-Nielson model" or the "*n*-modified Murray-Davies equation" is the earliest model that accounts for the Yule-Nielson effect. It is an empirical model that models the non-linear relationship between R and F Yule and Nielson developed the model by experimenting on different substrates which were coated and uncoated paper, opal glass (scattered light greatly), and aluminum (scattered light very little). Paper had a scattering efficiency between opal glass and aluminum. Yule and Nielson found that the nonlinear relationship between R and F followed the following mathematical relationship.

$$R^{1/n} = F(R_i)^{1/n} + (1 - F)(R_p)^{1/n} \tag{3.7.1}$$

The n factor is used to account for the nonlinearity and is traditionally determined by experimentally fitting the equation to R vs. F data. Theoretically, n maintains a value between 1.0 and 2.0 but empirically n can be larger than 2.0. When n approaches infinity, the optical density (D = -log R) and F becomes linear.[14]

The Yule-Nielson equation does not fundamentally describe the individual physical and optical behaviors of the halftone pattern. The n factor is a function of the spatial frequency of the halftone dot pattern and the optical and spatial properties of the ink and paper system.[13] Also, the Yule-Nielson equation does not describe the inherent nature of the paper and ink system. Photon flux (essentially reflectance) should add

linearly as suggested by the Murray-Davies equation as opposed to the power factor of $1/n$.[15] Hence, the Yule-Nielson equation does perform well in modeling the relationship between R and F but fails in describing the true optics and physics of the paper and ink system.

3.8 Arney-Katsube Probability Model

The Arney-Katsube Probability Model[1,2] is an empirical model that not only describes the nonlinear relationship between R and F but also the relationship between R_p with F and R_i, with F The model's parameters, unlike the n factor in the Yule-Nielson model, are related to individual physical and optical properties of the paper and ink system.

The most fundamental approach to modeling the Yule-Nielson effect is to perform a convolution between the paper's PSF (eq. 3.2.1) and the geometric pattern of the halftone dot, G(x,y).[16,17,18,19] This approach may be computationally intensive and would be difficult to implement when considering three dimensional effects such as ink penetration, non-uniform ink coverage, ink spread, and etc. The advantage the Probability Model has over the convolution approach is that its parameters can provide a more descriptive analysis of the tone reproduction system and the system can be represented by simple algebraic equations.

Certain assumptions are made in order to simplify the derivation of the Probability Model. These are that there is no ink penetration (perfect hold-out), no scattering of light occurs inside the dot (Beer-Lambert theory applies), and the contribution between the internal reflectances of the paper and the dot are considered to be negligible. The model was tested on samples which consisted of film with high density dots placed in vacuum contact on top of the paper. These dots simulated what

will be called simple dots (zero transmittance, sharp edges, and perfect holdout). The model was developed for five different halftone geometries: AM lines, AM dots, FM lines, FM spaces, and stochastic.

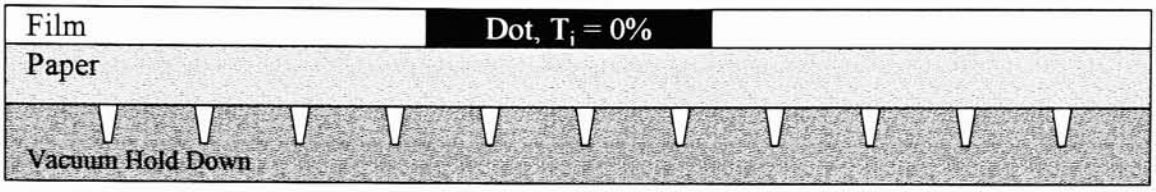

Figure 3.8.1: Test sample used to test the Probability model which simulated a simple dot (zero transmittance, sharp edges, and perfect holdout).

The Probability Model operates on probability functions that describe the lateral scatter of light in the paper.[1,21,23] One probability function, P_p, describes that the probability that a photon that enters the paper between the halftone dots will emerge from the paper beneath a halftone dot.[1]

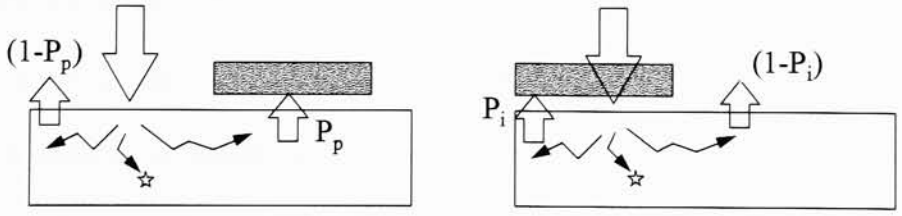

Figure 3.8.2: The Probability Model models the lateral scatter of light in the paper as a probability of where the light would emerge. The parameter P_p represents the the probability of light entering the paper between the dots emerges under a dot. P_i represents the light that enters the paper through a dot emerges under a dot.

The reflectance of the paper between the dots is dependent on this probability function.

$$R_p = R_g\left[1 - P_p\left(1 - T_i\right)\right] \tag{3.8.1}$$

R_g is the reflectance of the non-printed portion of the paper and T_i is the transmittance of the ink. Both terms are constants and are independent of F.

Another probability function, P_i, is the probability that a photon entering the paper from the dot exits from the paper below the dot. It was shown that both probabilities, P_p and P_i, are related by the following equation.

$$P_i = 1 - P_p \cdot \left(\frac{1-F}{F}\right) \tag{3.8.2}$$

Like R_p, the ink reflectance, R_i, is dependent on P_i.[1]

$$R_i = R_g T_i\left[1 - P_i\left(1 - T_i\right)\right] \tag{3.8.3}$$

Using the Murray-Davies model and not having R_i and R_p to be constant, the total reflectance of the halftone pattern is calculated using eq. 3.8.1, $R = FR_i + (1 - F)R_P$. The form of the equation for P_p was dependent on the halftone geometry. The equations for P_p were empirically determined for each halftone geometry and the equations are displayed in table 3.8.1.[2] The w parameter is a quantitative index that measures the magnitude of the Yule-Nielson effect. It has been determined to be exponentially

dependent on the product of the paper MTF constant, k_p (in units of mm), and the screen frequency of the halftone pattern, f (in units of mm^{-1}).[15]

$$w = 1 - e^{-Ak_p f} \tag{3.8.4}$$

A and B are empirical constants for calibrating w and P_p for each halftone geometry.

Halftone Geometry	A	B	Equation
AM Lines	0.48	--	$P_p = F[1-(1-F)^w+(1-F^w)]$
AM Dots	0.48	--	$P_p = F[1-(1-F)^w+(1-F^w)]$
FM Lines	0.24	--	$P_p = F[1-(1-F)^w+(1-F^w)]$
FM Spaces	0.13	2.0	$P_p = w[1 - (1 - F)^B]$
Stochastic	0.24	1.2	$P_p = w[1 - (1 \quad F)^B]$

Table 3.8.1: Empirical equations for P_p for each type of halftone geometry.

3.8.1 Procedure for applying the Arney-Katsube Probability Model

(1) Input Parameters

(A) Measure:
T_i: ink transmittance
R_g: reflectance of the unprinted portion of the paper

(B) Adjust w to fit measured plots of R_i vs. F, R_p vs. F, and R vs. F This is done by applying the following equations of the model in the following sequence.

(2) Probability Model's equations:
Start with F and do the following, in sequence.

(A) $P_p = F[1-(1-F)^w + (1-F^w)]$ or P_p=w[1-(1-F)^B] (table 3.8.1)
depending on the halftone geometry

(B) $$P_i = 1 - P_p \cdot \left(\frac{1-F}{F}\right) \quad (3.8.2)$$

(C) $$R_p = R_g\left[1 - P_p(1 - T_i)\right] \text{ (plot vs. } F) \quad (3.8.1)$$

(D) $$R_i = R_g T_i \cdot \left[1 - P_i \cdot (1 - T_i)\right] \text{(plot vs. } F) \quad (3.8.3)$$

(E) $$R = R_i \cdot F + R_p \cdot (1-F) \text{ (plot vs. } F) \quad (3.6.1)$$

3.9 Modified Probability Model

The Probability Model provided an algebraic explanation of tone reproduction considering optical dot gain. The model was designed from simple halftone dots which consisted of perfect hold-out, high optical density, and sharp edges. To modify the model so that it accounts for ink spread and ink penetration, the modification will be broken down into two parts. It will first be modified for ink spread and then it will be modified further for ink penetration.

3.9.1 Modeling Ink Spread

To adjust the Probability Model for ink spread, it must consider the effects ink spread has on a halftone dot. Ink spread causes a dot to be larger in size and to be less dark. The parameters in the Probability Model to be mathematically adjusted to simulate these effects are the dot area fraction, F, and the ink transmittance, T_i.

3.9.1.1 Modeling the Effect Ink Spread has on F

The approach to model the effect ink spread has on F was done by relating the device's ideal dot area fraction, F_o, to the actual dot area fraction, F As mentioned in section 3.1, the relation of F_o to F is affected by the dot size and the placement of the dots. A large dot size causes F to be larger than F_o and a smaller dot size causes F to be smaller than F_o. The misplacement of the ink jet dots due to the misalignment of ink

cartridges may make F either larger or smaller than F_o. The misplacement of ink jet dots would be unpredictable and would be difficult to model using a first principles approach. Therefore, a mathematical model relating F vs. F_o was developed empirically. Data was collected consisting of F_o and F and a simple power function was chosen to fit the data. The power function chosen will be discussed in section 4.5.

3.9.1.2 Modeling the Effect Ink Spread has on T_i

To derive an equation that will simulate the effect ink spread has on T_i, an ideal dot was assumed that would have sharp edges, perfect hold-out, and would be transparent. It would be assumed that it obeyed Beer-Lambert theory and thus, it would be called a Beer-Lambert dot. The background reflectance was assumed to be zero. The contribution of light from the internal reflectance between the dot and the paper was considered to be negligible. For ink spread, it was assumed that the volume of the dot was constant but the dot area, A, and the dot thickness, x, would change.

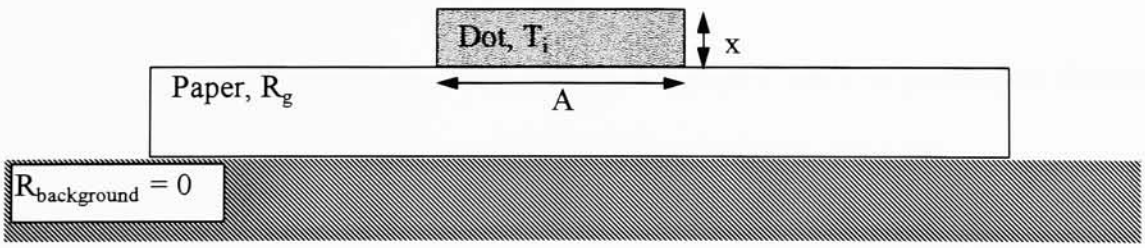

Figure 3.9.1: An ideal dot model (Beer-Lambert dot) that was used in the derivation in modeling ink spread.

The transmittance of the dot from Beer-Lambert theory as mentioned in section 3.2 was chosen to be the following equation.

$$T_i = 10^{-\varepsilon C x} \tag{3.9.1}$$

where, ε: extinction coefficient (in units of m^2/g)

C: concentration of colorant in the dot (in units of g/m^2)

x: thickness of the dot (in units of meters)

(Note: The final form of the Modified Probability Model uses the Kubelka-Munk transmittance equation (as shown in section 3.9.2.1). The Beer-Lambert transmittance equation is used in deriving an equation that would use parameters that can be easily measured and to be included into the Kubelka-Munk transmittance equation.)

Since C and x have a true physical meaning, ε actually depends on how efficient the colorant absorbs photons. The greater the efficiency, the greater ε is and therefore, the lower the ink transmittance. Hence, ε can be used as a metric for measuring the light absorbing efficiency of the colorant. The value for ε will be obtained empirically by adjusting its value so the model fits the data.

For the experimentation, it was decided to replace C and x by parameters that are easier to measure. What follows are the derivations to alter eq. 3.9.1 for experimentation.

To make eq. 3.9.1 easier to use for experimentation, the concentration must be defined. The concentration, C, is defined as g grams of the colorant divided by the volume of the dot.

$$C = \frac{g}{Ax} \tag{3.9.2}$$

By substituting C (eq. 3.9.2) into the transmittance equation (eq. 3.9.1) gives the following equation.

$$T_i = 10^{\frac{-\varepsilon g}{A}} \tag{3.9.3}$$

The dot area fraction is defined as the area of the dot, A, over the area the dot could cover, A_o.

$$F = \frac{A}{A_o} \text{ which gives } A = FA_o \tag{3.9.4}$$

A_o is actually the area the dot would cover if it spreads out so the dot area fraction would be 100% (as shown in figure 3.9.2).

By placing A (eq. 3.9.4) into T_i (eq. 3.9.3), the following is the resulting equation.

$$T_i = 10^{\frac{-\varepsilon g}{A_o F}} \tag{3.9.5}$$

Next what will be defined is the ink coverage. The ink coverage, C_c, will be

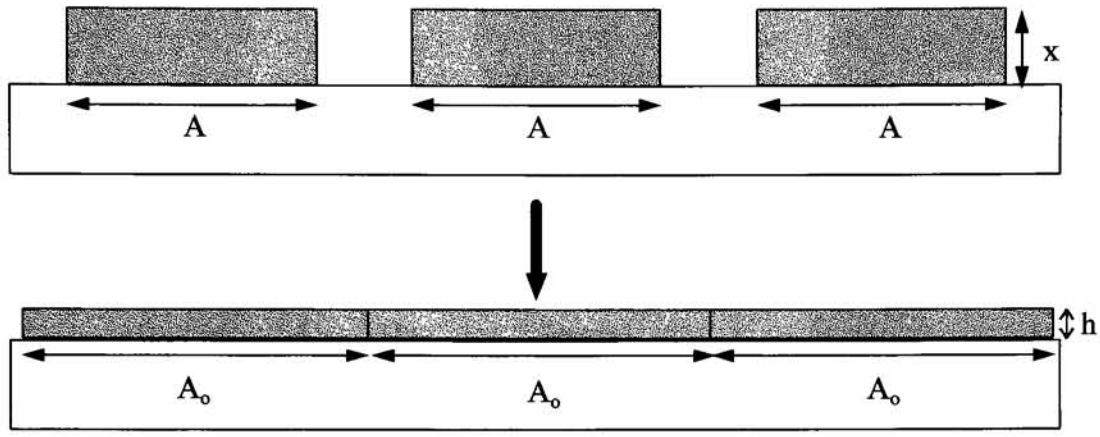

Figure 3.9.2: Portrayal illustrating if a dot of area, A, spreads out to an area, A_o, to occupy 100% dot area fraction.

defined as g grams of the colorant in the dot divided by A_o area the dot could occupy.

$$C_c = \frac{g}{A_o} \tag{3.9.6}$$

Placing this equation into eq. 3.9.5 gives the next equation for T_i.

$$T_i = 10^{\frac{-gC_c}{F}} \tag{3.9.7}$$

C_c can be empirically obtained by measuring the number of grams of ink laid down, kg (where k is the number of drops of ink laid down), divided by the area the pattern covers, A_m. A_m is defined as the number of drops of ink, k, times the area of 100% dot spread, A_o.

$$A_m = kA_o \tag{3.9.8}$$

Therefore, C_c will now be the following.

$$C_c = \frac{kg}{A_m} \tag{3.9.9}$$

The maximum ink coverage, C_o, the ink jet printer can cover is defined as the maximum amount of grams of ink laid down, mg (where m is the maximum number of drops of ink laid down), divided by the area the pattern covers, A_m.

$$C_o = \frac{mg}{A_m} \tag{3.9.10}$$

Substituting C_o (eq. 3.9.10) into C_c gives the following equation.

$$C_c = C_o \frac{k}{m} \tag{3.9.11}$$

F_o will be defined as the ink jet printer's ideal dot area fraction. It will be the number of drops of ink laid down, k, divided by the maximum number of drops, m.

$$F_o = \frac{k}{m} \tag{3.9.12}$$

Placed into eq. 3.9.11 gives the equation for C_c.

$$C_c = C_o F_o \tag{3.9.13}$$

Substituting into T_i (eq. 3.9.7), gives the final form of T_i.

$$T_i = 10^{-\frac{\varepsilon C_o F_o}{F}} \tag{3.9.14}$$

Thus, T_i is now in a form of which it is represented by parameters that are more suitable for experimentation. ε will be obtained empirically from the data. C_o will be

measured by printing the darkest halftone pattern and measuring the grams and area of the pattern. F_o will be determined by the value the computer instructs the printer to print at. The parameter F will be determined from microdensitometry equipment.

Hence, by including the equations for F (to be empirically determined) and T_i (eq. 3.9.14) into the Probability Model, the Probability Model will be able to account for ink spread.

3.9.2 Modeling Ink Penetration

In the last section the Probability Model was modified to consider ink spread; it will now be further modified to consider ink penetration. To model ink penetration, the dot will be modeled as if it scatters light. Beer-Lambert theory will be ineffective for these derivations since it only considers the absorption of light by the colorants. Kubelka-Munk theory is more effective since it not only considers the absorption of light but also the scattering of light. It will be used in place of Beer-Lambert theory in these derivations.

For these derivations, ink penetration will be modeled by using the same ideal dot model used in section 3.9.1.2 except the dot will scatter light. This type of dot will be known as a Kubelka-Munk Dot.

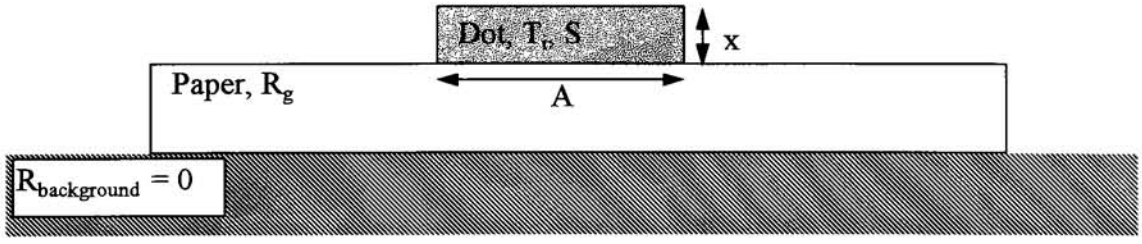

Figure 3.9.3: An ideal dot model (Kubelka-Munk dot) that was used in the derivation of modeling ink penetration. It is the same dot model used in section 3.9.1.2 except the dot scatters light (represented by variable *S*).

3.9.2.1 Modeling the Effect Ink Penetration has on T_i

The transmittance of the Kubelka-Munk dot is the following transmittance equation from Kubelka-Munk theory. This transmittance equation replaces eq. 3.9.14

$$T_i = \frac{b}{a \cdot Sinh(bSx) + b \cdot Cosh(bSx)} \tag{3.9.15}$$

$$a = \frac{S+K}{S} \tag{3.9.16}$$

$$b = \sqrt{a^2 - 1} \tag{3.9.17}$$

where, S: scattering coefficient (no units)

K: absorption coefficient (no units)

x: thickness of the ink film (in units of meters)

The product Sx in eq. 3.9.15will be treated as a single term. The value of Sx will be obtained empirically by fitting the model to data. Sx will be expected to increase for ink penetration since the scattering of the paper would cause S to increase.

The right hand side of the equation for a will be multiplied by x so that the Sx term will appear in the equation.

$$a = \frac{Sx + Kx}{Sx} \tag{3.9.18}$$

From Kubelka-Munk theory, K is known to have the following relation.

$$K = 2.303\varepsilon C \tag{3.9.19}$$

Since the Kx term is found in a (eq. 3.9.18), eq. 3.9.19 will be multiplied by x.

$$Kx = 2.303\varepsilon Cx \tag{3.9.20}$$

It is observed that εCx is in eq. 3.9.1. Since eq. 3.9.1 and eq. 3.9.14 are equal, the following relations are set equal.

$$\varepsilon Cx = \frac{\varepsilon C_o F_o}{F} \tag{3.9.21}$$

Substituting εCx (eq. 3.9.21) into Kx (eq. 3.9.20) gives the following equation for Kx.

$$Kx = 2.303\varepsilon C_o \frac{F_o}{F} \tag{3.9.22}$$

The value for the ink transmittance (eq. 3.9.15) is therefore determined by the values of Kx and Sx. Sx will be obtained empirically and Kx will be obtained by eq. 3.9.22.

3.9.2.2 Modeling the Effect Ink Penetration has on R_i and R_p

For paper reflectance, R_p will be the same equation as in the Probability Model (eq. 3.8.1) except the new equation for T_i (eq. 3.9.15) will be used.

$$R_p = R_g\left[1 - P_p\left(1 - T_i\right)\right] \tag{3.9.23}$$

For ink reflectance, R_i will be considered to be composed of two components. The first component, R_{i1}, consists of the light underneath the dot that is transmitted through the dot (see figure 3.9.4). The equation for this component is taken from the Probability Model (eq. 3.8.3).

$$R_{i1} = R_g T_i \cdot \left[1 - P_i \cdot \left(1 - T_i\right)\right] \tag{3.9.24}$$

As shown in figure 3.9.4, when light enters into the dot it can be scattered out of the dot (I_3), absorbed by the dot (I_2), or transmitted (I_1) through the dot. The second reflectance component, R_{i2}, consists of the light that is scattered out of the dot (I_3) divided by the light that enters into the dot from the top (I_o). Since I_3 is the portion of light that is scattered out of the dot, this portion of light never reaches the paper. Thus, R_{i2} is unaffected by the paper and is described by the Kubelka-Munk function for $R_g = 0$.

$$R_{i2} = \frac{1}{a + b \cdot Coth(bSx)} \tag{3.9.25}$$

R_i is then the addition of the two reflectance components.

$$R_i = R_{i1} + R_{i2} \tag{3.9.26}$$

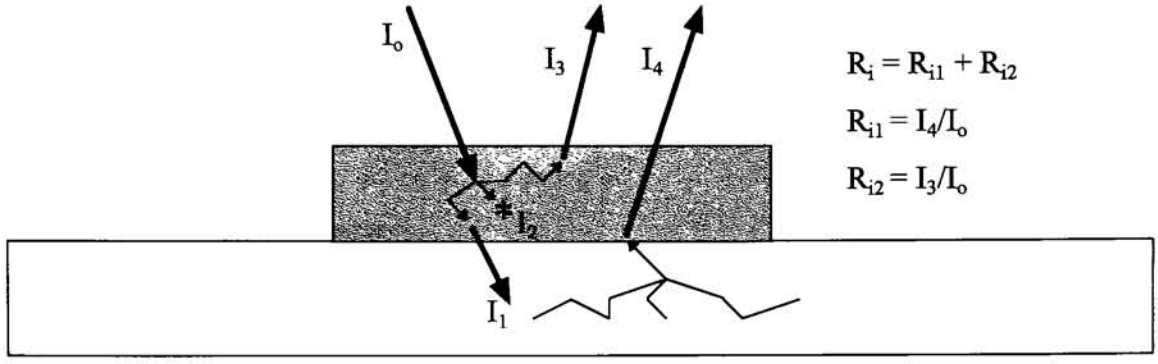

Figure 3.9.4: When light enters into the Kubelka-Munk dot, it can be scattered out of the dot (I_3), absorbed by the dot (I_2), or transmitted (I_1) through the dot The reflectance of the Kubelka-Munk dot consists of two components, R_{i1} and R_{i2}. R_{i1} consists of all the light in the paper under the dot (I_4) that transmits through the dot. R_{i2} consists of the light that scatters out of the dot (I_3).

3.9.2.3 Modeling the Effect Ink Penetration has on P_p

P_p is the probability that the light entering between the dots would emerge from beneath the dots. For a Beer-Lambert dot which does not scatter light, the light beneath the dot would transmit through unaffected. For a Kubelka-Munk dot, some of the light from beneath the dot would scatter back into the paper and re-emerge between the dots. This would have an affect on the value of P_p by causing its value to decrease.

For no scattering of light inside the dot (S=0), P_{po} will be defined as one of the two equations chosen from the table in the Probability Model (table 3.8.1).

$$P_{po} = F[1-(1-F)^w + (1-F^w)] \text{ or } P_{po}=w[1-(1-F)^B] \qquad (3.9.27)$$

P_{po} can be looked at as the fraction of photons from between the dots that are emerging underneath the Kubelka-Munk dots. The fraction of the photons that emerge through the Kubelka-Munk dot can be observed as being 1-R_{i2}. R_{i2} is the reflectance of a Kubelka-Munk dot over a black background (R_g = 0) which will be derived in the next section from Kubelka-Munk theory. The background is considered to be black since the

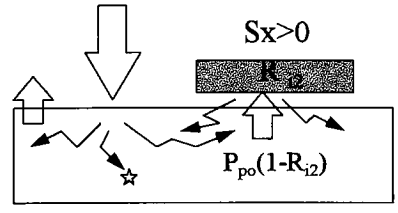

Figure 3.9.5: For a Kubelka-Munk dot, a fraction of the light that emerges under the dot is scattered back into the paper. The fraction that scatters back into the paper is the reflectance R_{i2}. This causes the probability parameter P_p to decrease.

photons are incident on the bottom of the dot and the background would be considered to be the top of the dot. Hence, P_p for a dot that scatters light would be the product of P_{po} and 1-R_{i2}.

$$P_p = P_{p_o}\left[1 - R_{i2}\right] \tag{3.9.28}$$

This equation for P_p is to be included in the R_{i1} equation (eq. 3.9.24) and the P_i equation (eq. 3.8.2).

3.9.3 Procedure for applying the Modified Probability Model

(1) Input Parameters

(A) Measure:

C_o : maximum ink coverage of the ink

R_g : reflectance of the unprinted portion of the paper

(B) Calibrate the F vs. F_o equation for the printing condition.

(C) Adjust ε, w, and Sx to fit measured plots of R_i vs. F, R_p vs. F, and R vs. F This is done by applying the following equations of the model in the following sequence.

(2) The Model equations:

Start with F and do the following, in sequence.

(A) $Kx = 2.303\varepsilon C_a \dfrac{F_o}{F}$ (3.9.22)

(B) $a = \dfrac{Sx + Kx}{Sx}$ (3.9.16)

(C) $b = \sqrt{a^2 - 1}$ (3.9.17)

(D) $T_i = \dfrac{b}{a \cdot Sinh(bSx) + b \cdot Cosh(bSx)}$ (3.9.15)

(E) $P_{po} = F[1-(1-F)^w + (1-F^w)]$ or $P_{po}=w[1-(1-F)^B]$ (3.9.27)

depending on the halftone geometry chosen from table 3.9.1

(F) $R_{i2} = \dfrac{1}{a + b \cdot Coth(bSx)}$ (3.9.25)

(G) $P_p = P_{p_o}\left[1 - R_{i2}\right]$ (3.9.28)

(H) $P_i = 1 - P_p \cdot \left(\frac{1-F}{F}\right)$ (3.8.2)

(I) $R_{i1} = R_g T_i \cdot \left[1 - P_i \cdot (1 - T_i)\right]$ (3.9.24)

(J) $R_i = R_{i1} + R_{i2}$ (plot vs. F) (3.9.26)

(K) $R_p = R_g\left[1 - P_p(1 - T_i)\right]$ (plot vs. F) (3.8.1)

(L) $R = R_i \cdot F + R_p \cdot (1 - F)$ (plot vs. F) (3.6.1)

4. Approach

To test the Modified Probability Model for its validity, test samples were developed that consisted of a grey scale pattern printed by ink jet under different printing conditions that affected the ink penetration, ink spread, and simulated other ink jet environments. For each gray scale test sample, image microstructure data (R, R_i, R_p, and F) were measured through use of microdensitometry equipment. F_o was obtained from the printer command sent to the printer. After viewing the characteristics of F vs. F_o data, empirical F vs. F_o equations were developed. The F vs. F_o equations were calibrated for each test sample. The Modified Probability Model's R_i vs. F, R_p vs. F, and R vs. F equations were then fitted to the R_i vs. F, R_p vs. F, and R vs. F data by adjusting parameters ε, w, and Sx. The model will be examined on how well it is able to model image microstructure tone reproduction data and if the parameters Sx and ε explain the effects the printing conditions have on the inherent properties of the ink.

4.1 Discussion of Test Samples Produced

To test the model, test samples were produced that consisted of a gray scale printed by an ink jet printer. Two ink jet printers from different manufacturers were used. The manufacturer of one printer was Hewlett-Packard and the printer was a HP1600C deskjet. The manufacturer of the other printer was ENCAD with the model of the printer unknown since the test samples were developed outside the research facility (test samples were produced by a chemical company). The test samples printed by these printers are displayed in figure 4.1.1.

The tones of the HP1600C were controlled using a gray level, G. G set at zero gave the darkest tone and G set at 255 gave the lightest tone (no ink on paper). A program was written using the printer control language, *PCL5*, to program the HP1600C to print a grey scale test pattern. For the test samples produced by the ENCAD printer, the test samples received by the chemical company did not display the tones as grey levels but as dot area fractions.

The test samples produced were designed to have different degrees of ink spread and ink penetration and to simulate other ink jet and ink-paper environments that are thought to have an effect on dot gain. The type of halftone geometry chosen for making the test samples was a disperse dot halftone.

To control ink penetration in the test samples, an uncoated paper with poor hold-out and a synthetic paper with good hold-out was used. To control ink spread, ink with

and without surfactant was used. Surfactant is a chemical agent that helps to cause the ink to spread.

For simulating other ink-paper environments, a dye-based and a pigment-based ink were used and a different brand of synthetic and uncoated paper were used. Also, a two color overprint at 100% yellow and varying magenta was used. The two color overprint test sample was developed on the HP1600C printer with the grey level of yellow set at 0 and the magenta grey level varied. The colorant for the yellow ink was a dye and the colorant for the magenta ink was a pigment. For simulating other ink-jet environments, different ink jet printers were utilized. As mentioned, a Hewlett-Packard HP1600C printer and an ENCAD printer were used.

The HP1600C has a heating element. The heating element causes the ink to evaporate more quickly. The heating element was designed to help prevent dots from mixing (which is important in color printing) and prevent the paper from cockling. Cockling is the puckering of paper caused by the aqueous nature of the ink.[4,23] Since the ink in the halftone dots would be affected by the application of heat, samples were produced by the HP1600C with the heat on and off.

Table 4.1.1 displays all the test samples and their printing condition s. After producing the test samples, it was observed by using a line scan, a one dimensional scan of optical density vs. distance across halftone dots (technique described in section 4.5),

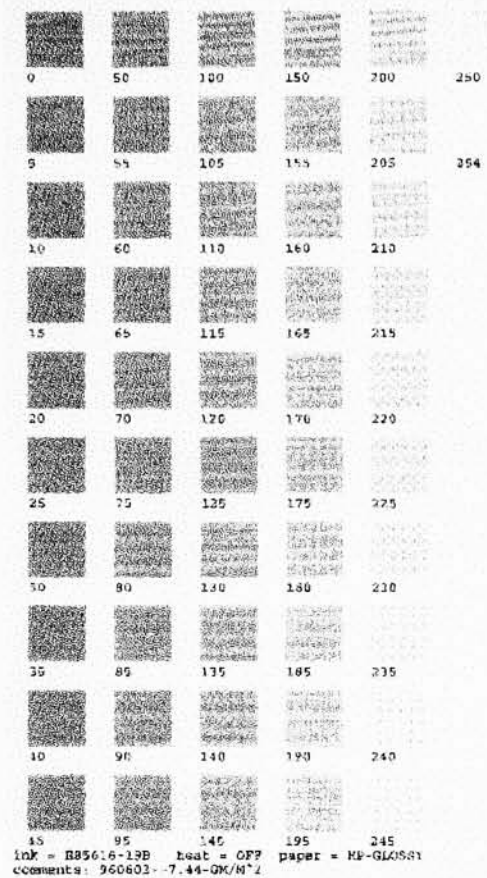

(a) HP1600C test sample

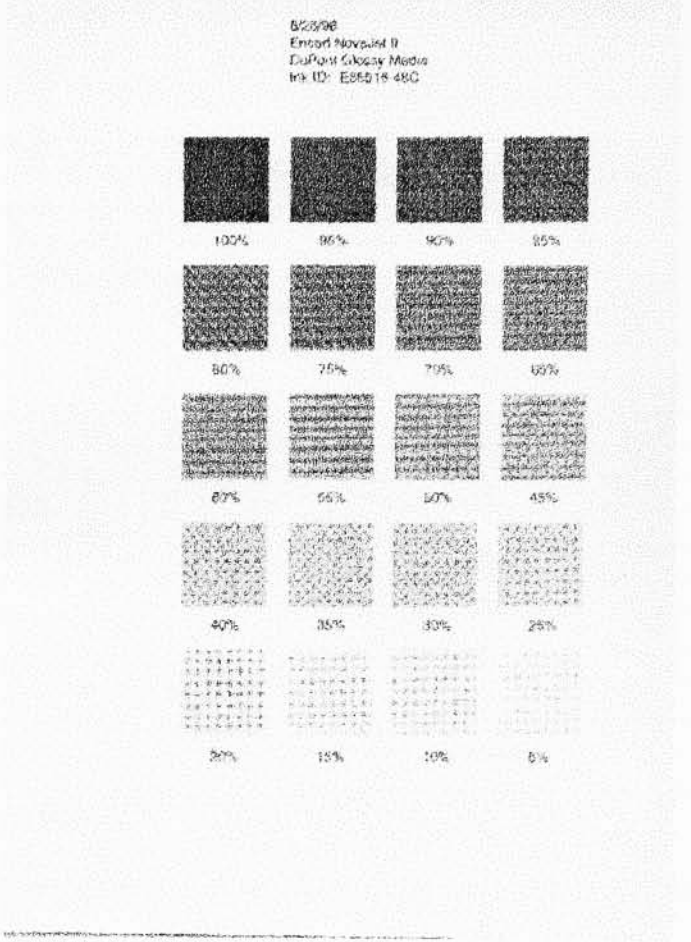

(b) ENCAD test sample

Figure 4.1.1: Images of test samples produced.

	Pigmented ink		Dyed ink	Paper		Heat		Ink Jet Printer		
Sample	without surfactant	with surfactant	without surfactant	uncoated	synthetic	not applied	applied	HP1600C	ENCAD	C_o
1	x			x		x		x		7.31
2	x				x	x		x		7.31
3		x		x		x		x		7.47
4		x			x	x		x		7.47
5	x			x			x	x		7.31
6	x				x		x	x		7.31
7		x		x			x	x		7.47
8		x			x		x	x		7.47
9			x	x		x		x		7.14
10			x		x	x		x		7.14
11			x	x			x	x		7.14
12			x		x		x	x		7.14
13	x			x		unknown	unknown		x	7.4[#]
14	x				x	unknown	unknown		x	7.4[#]
15		x		x		unknown	unknown		x	7.4[#]
16		x			x	unknown	unknown		x	7.4[#]
17*	x		x	x		x		x		7.31
18*	x		x		x	x		x		7.31
19*		x	x	x		x		x		7.31
20*		x	x		x		x	x		7.31

Table 4.1.1: Table of printing conditions of the test samples produced.

**Samples 17-20:* Two color overprint samples: dyed yellow ink set at grey level equal to 0 with magenta pigmented inks printed with grey level varying from 0 to 255.

[#]*Samples 13-16:* Test samples were produced outside of facility (produced by a chemical company). C_o values were not given. An assumed value of 7.4 was used for C_o.

Test Patterns' Halftone Geometry: Disperse Dot Halftone

	uncoated paper		synthetic paper	
printer	brand name	R_z	brand name	R_z
HP1600C	Hammermill Unity DP Recycled	0.68	Hewlett-Packard Ink Jet Glossy	0.81
ENCAD	Weyerhaeuser Laser Copy Premium Xerox	0.79	DuPont Glossy Media	0.81

Table 4.1.2: Brand Names and Reflectance Values of Papers

pigmented ink	dyed ink
proprietary ink jet ink supplied by a chemical co. -- magenta	Hewlett Packard -- magenta and yellow

Table 4.1.3: Description of Inks

that the synthetic paper produced a darker, more well defined halftone dot than uncoated paper as illustrated in figure 4.1.2.

Surfactant seemed to affect the halftone dots the most when heat was applied as

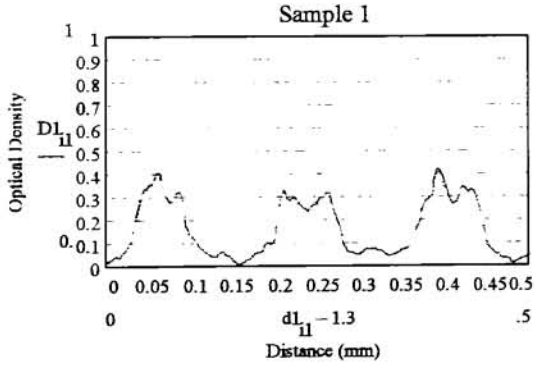

grey level = 190
(a) uncoated paper

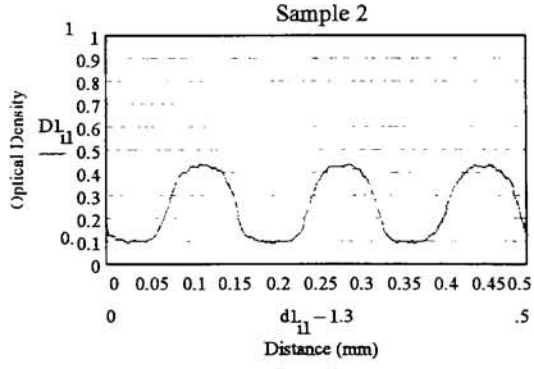

grey level = 190
(b) synthetic paper

Figure 4.1.2: Line scans of uncoated paper displayed that the dots were more defined and darker than dots produced on synthetic paper.

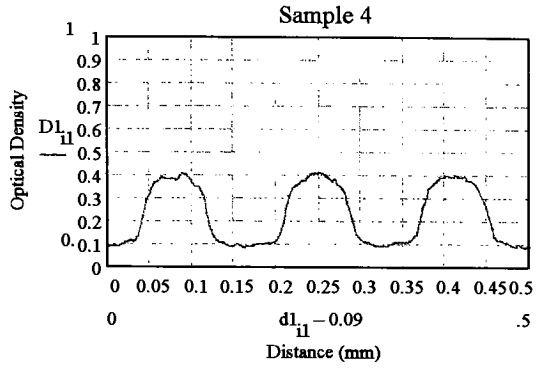

grey level = 190
(a) surfactant with heat off

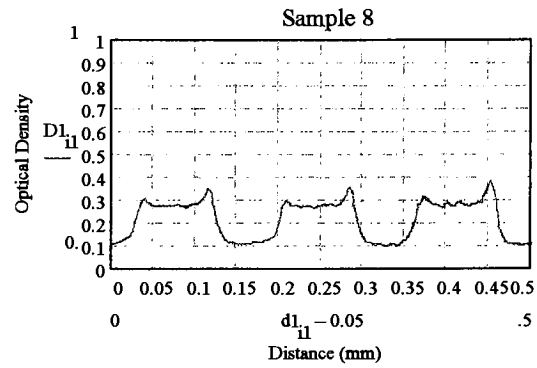

grey level = 190
(b) surfactant with heat on

Figure 4.1.3: The surfactant used seemed to affect the dots the most when heat was applied.

displayed in figure 4.1.3. Surfactant caused the halftone dots to have a dark rim on the edge of the dot.

The halftone dots produced by the ENCAD printer were larger than the HP1600C printer as illustrated in figure 4.1.4.

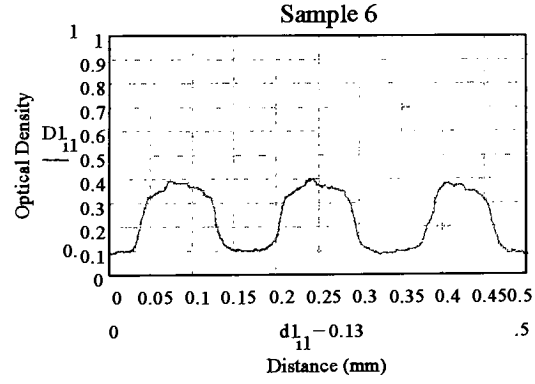

grey level = 190
(a) HP1600C

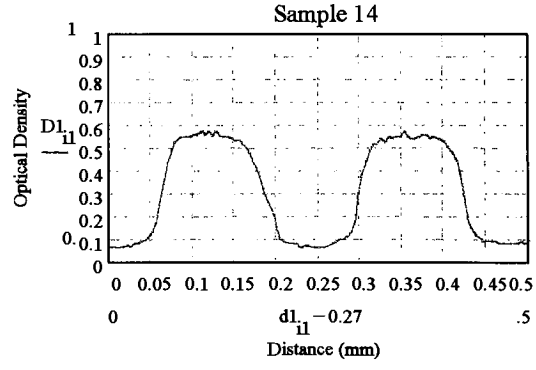

dot area fraction command = 35%
(b) ENCAD

Figure 4.1.4: The halftone dots produced by the ENCAD printer were larger than the dots produced by the HP1600C.

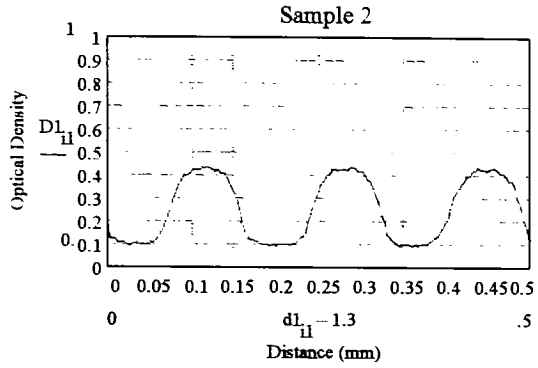

grey level = 190
(a) pigmented ink

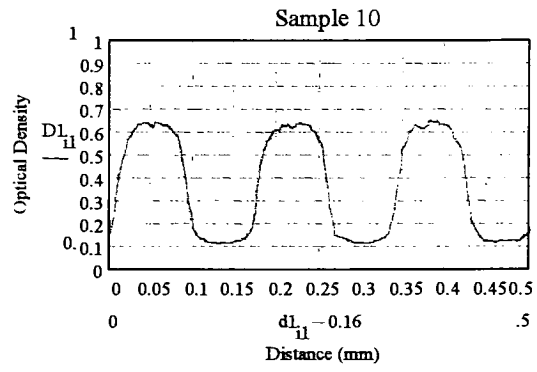

grey level = 190
(b) dyed ink

Figure 4.1.5: The dyed ink produced a darker dot than the pigmented ink.

The dyed ink produced a darker dot than the pigmented ink as shown in figure 4.1.5. For two color overprints, magenta dots and yellow dots overlapped one another causing the magenta dots to be distorted as displayed in figure 4.1.6.

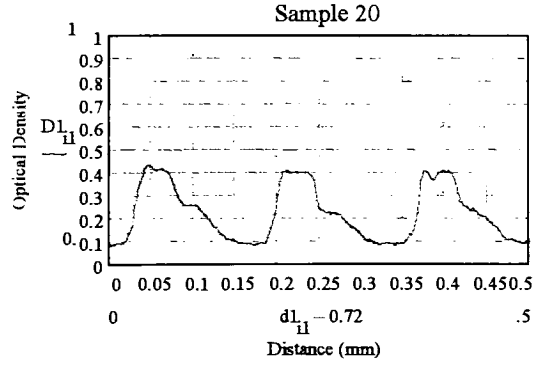

magenta grey level = 190, yellow grey level = 0
(a) two color overprint on coated paper

Figure 4.1.6: Magenta dots were distorted for a two color overprint due to the magenta dots and yellow dots overlapping one another.

For two color overprints (yellow dots and magenta dots) on uncoated paper (samples 17 and 19), the uncoated paper was more wet than the uncoated paper for a single color print (magenta dots) since the yellow ink was printed at a grey level equal to zero (100% dot area fraction). This caused the magenta halftone dots to be very distorted and washed out as illustrated in figure 4.1.7.

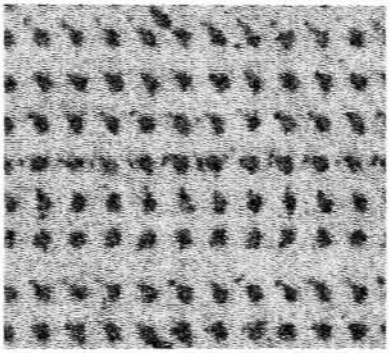

sample 2
magenta grey level = 190

(a) magenta dots
on uncoated paper

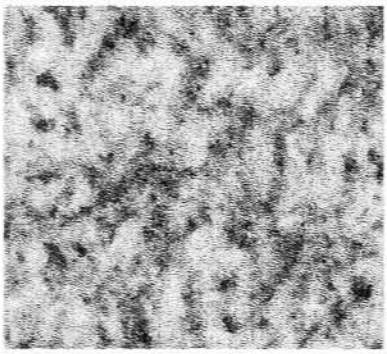

sample 17
magenta grey level = 190
yellow grey level = 0
(b) magenta dots and yellow dots
on uncoated paper

Figure 4.1.7: For two color overprints on uncoated paper, the magenta halftone dots appeared washed out and very distorted.

4.2 Technique for measuring Ink Coverage, C_o, and Paper Reflectance, R_g

Before using the Modified Probability Model, the parameters C_o and R_g must be measured. To measure C_o, the following procedure was used.

Procedure for measuring the Ink Spread Parameter, C_o

(1) Weigh the mass of the ink cartridge, g_1 , on a balance.

(2) Print ink on a sheet of paper at a gray level = 0 (darkest gray level) covering an 8 inch x 10.5 inch area (84 in.^{2} = 0.0542 m^2).

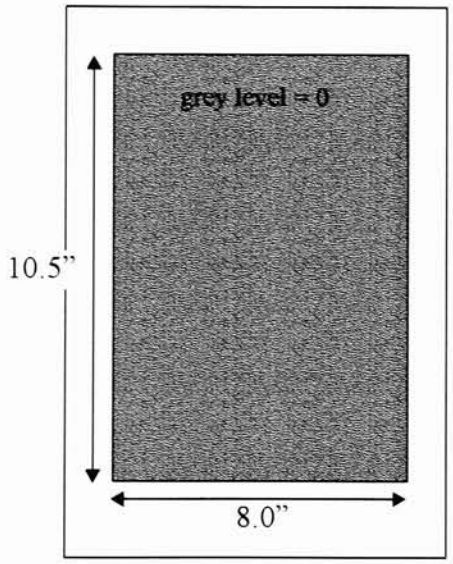

Figure 4.2.1: Diagram of the test sample used for measuring C_o.

(3) Weigh the mass of the ink cartridge after printing the 8 inch x 10.5 inch area, g_2. on a balance. The mass of ink on the sheet of paper is calculated by the difference between g_2 and g_1.

$$g_{ink} = g_2 - g_1 \tag{4.2.1}$$

(4) C_o is calculated by the following equation:

$$C_o = g_{ink} / (0.0542\ \mathrm{m}^2) \tag{4.2.2}$$

Measured values of C_o are display in table 4.1.1. Since values for C_o were not supplied by the chemical company for the test samples developed on the ENCAD printer, an assumed value of 7.4 was used.

The reflectance of the paper, R_g , was measured using a densitometer with the paper placed on top of a black background. A density reading was obtained and was converted to reflectance. Measured values of R_g are displayed in table 4.1.2.

4.3 Description of Equipment used for measuring Image Microstructure Data

About the same technique used in a past study was utilized in measuring image microstructure data from each test sample.[17] The equipment used (which is called microdensitometry equipment) consisted of a CCD video camera (COHU model #4815-2000/0000, San Diego, CA) that was connected to a microscope that produced a digitized image of a microscopic view of a patch on the gray scale of the test sample of interest. An illustration of the equipment is shown in figure 4.3.1. The image field of view was 1.84 x 1.33 mm with a pixel resolution of 512 x 464 pixels. The test pattern was illuminated by a ring illuminator attached to the microscope's objective. A black sheet of paper with a rectangular hole that was larger than the field of view was placed on top of the test pattern so light outside of the object of interest would not enter into the microscope and contribute to flare. A black sheet of paper was placed underneath the test sample to absorb any light that was transmitted through the test sample. An air pump was used to keep the paper flat.

The light for the ring illuminator was filtered by an infrared blocking filter and a green filter. The infrared filter was needed since a CCD camera is more sensitive in the infrared range and for also reducing the spectrum of the light source to the visible range. The green filter was needed in order to highlight the magenta colored ink. The CCD camera was connected to a frame grabber board (Imaging Technology, OFG Rev. C,

Bedford, MA) inside the computer. *Image Lab* image processing software (Warner Frei, Santa Monica, CA) was used in digitizing a monochromatic image from the CCD camera. A pixel on the digitized image was 1 byte or 256 gray levels. For measuring image microstructure data, *Image Lab* was used for its capability of producing a histogram of the image which consisted of *counts* vs. *gray level*. *Image Lab* was also used for its line scans capability (as used in the figures in section 4.1) which consisted of a one dimensional scan of *grey level* vs. *pixel's position (x and y coordinates)*.

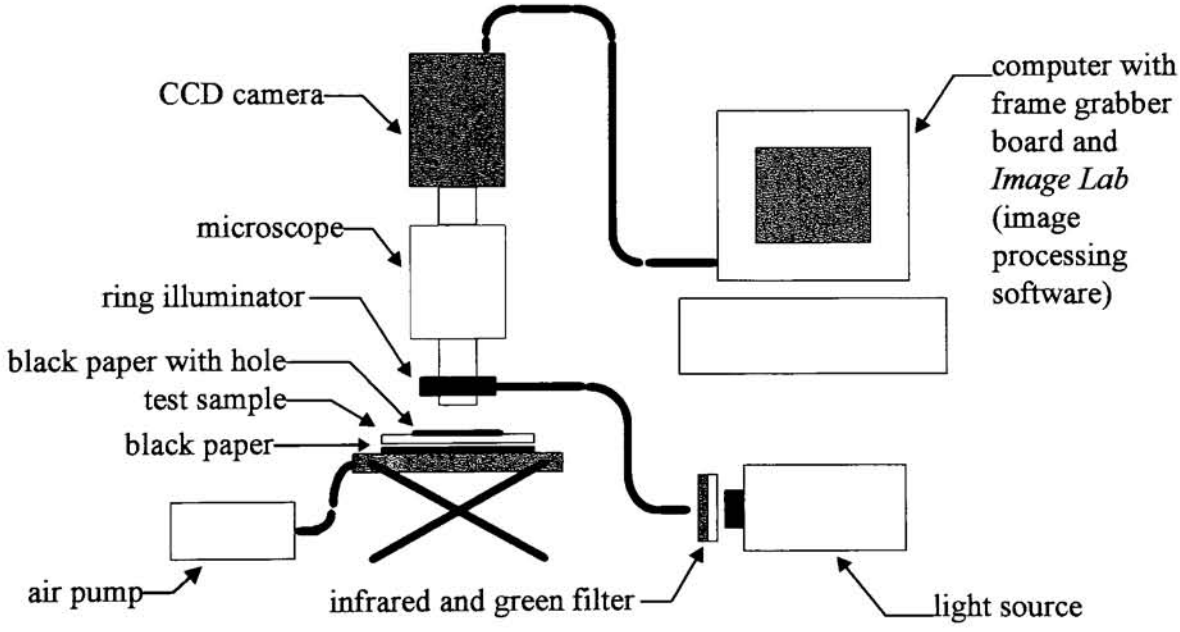

Figure 4.3.1: Illustration of microdensitometry equipment.

4.4 Technique for measuring Image Microstructure Data

To collect data for producing tone reproduction curves of R_i vs. F , R_p vs. F, and R vs. F from a grey scale ink jet test sample, measurements of R, R_i , R_p, and F were collected from eight to twelve halftone pattern patches at different dot area fractions. To measure the image microstructure data of one of the patches of a gray scale test sample, the data was obtained from the histogram of the digitized image of the patch. Figure 4.4.1 illustrates how the reflectances and dot area fraction were obtained. As mentioned in section 3.4, the histogram of a halftone pattern is bimodal with one peak representing R_i and the other peak representing R_p. Since *Image Lab* produced a histogram of counts vs. grey level, the grey level was converted to reflectance. The technique for converting the grey level to reflectance will be discussed later in the next paragraph. R_i was taken at the reflectance at the maximum value at the R_i peak and R_p was taken at the maximum value at the R_p peak. F was calculated by determining the area under the R_i peak up to the transition reflectance divided by the total area under the histogram.

As discussed in a past study, the gray level of a pixel from a CCD camera was found to be linear to the reflectance of the object the pixel was imaging (the linearity was tested in section 4.6).[13] To convert the gray level G to a reflectance factor, the gray level was calibrated against the lowest gray level value measured at the dark frame G_{dark} (which was the lens cap covering the microscope's objective lens) and against an average gray level value measured at the white frame G_{white} (which was the unprinted portion of

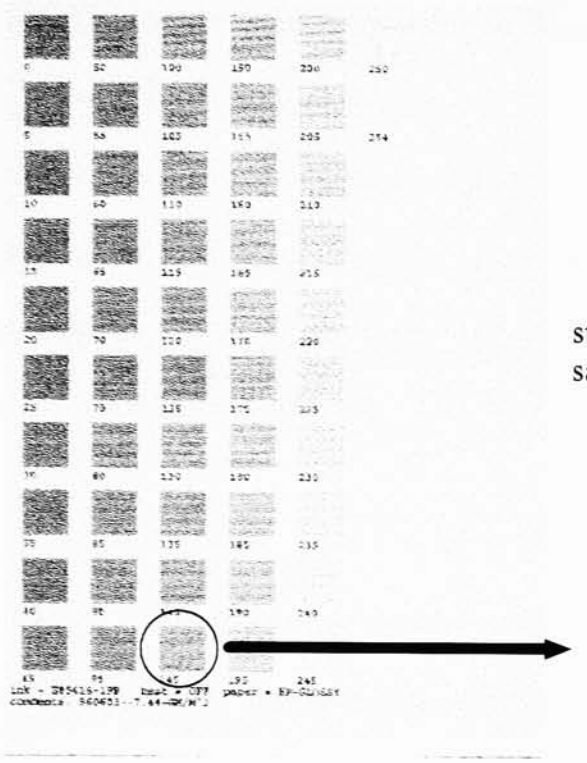

step 2: Digitized image of test sample

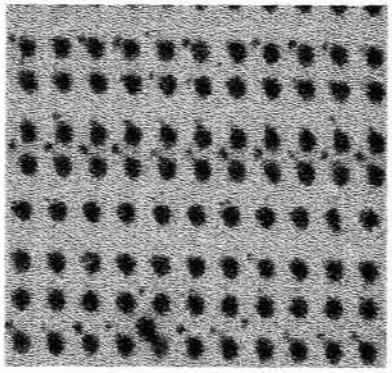

step 1: Chose patch from test sample.

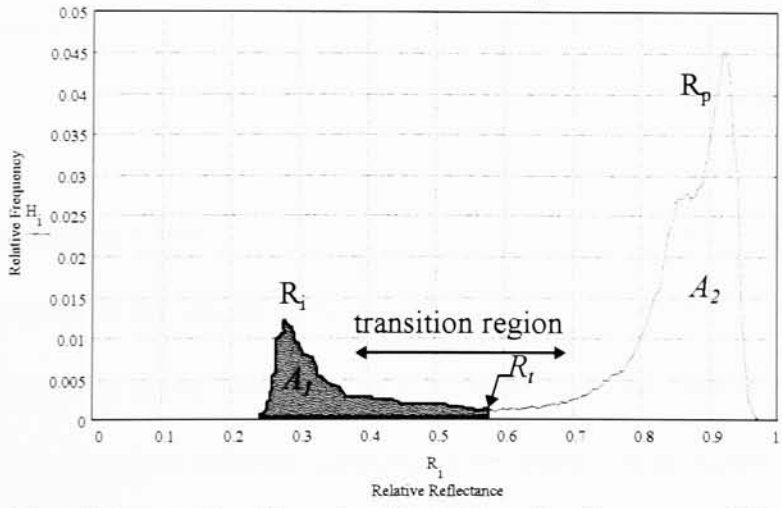

step 3: Obtained histogram of image and extrapolated image microstructure data.

$F = A_1/(A_1+A_2)$ $R_i = R_i$ peak $R_p = R_p$ peak R = mean of histogram

Figure 4.4.1: Illustration of how image microstructure data was obtained.

the paper). G_{dark} was measured by digitizing an image at the dark frame and obtaining the lowest grey level from the image histogram. G_{white} was measured by digitizing an image at the white frame and obtaining the average grey level from the image histogram. This reflectance was relative to the reflectance of the paper. It is common in the printing industry to measure reflectance relative to the paper's reflectance. The following was the equation for the relative reflectance.

$$R_{relative} = \frac{G - \min(G_{dark})}{avg(G_{white}) - \min(G_{dark})} = \frac{R_{object}}{R_{paper}} \tag{4.4.1}$$

Before obtaining image microstructure data, the digitized image of the halftone patch was corrected for the non-uniform illumination of the ring illuminator. This method was called flat fielding. A program was written to perform flat fielding on the image and was utilized through *Image Lab*. The program performed flat fielding by applying the following equation.

$$G_{flat}(x,y) = \frac{G(x,y) - G_{dark}}{G_{white}(x,y) - G_{dark}} \cdot [avg(G_{white}(x,y)) - G_{dark}] \tag{4.4.2}$$

For flat fielding, a white reference image, $G_{white}(x,y)$, of the paper was first taken. $G_{white}(x,y)$ was stored in the second memory register in *Image Lab* and the image to be flat fielded, $G(x,y)$, was stored in the first memory register. Eight images were taken for the white reference image at different locations on the paper and averaged so that the reflectance of the paper at a pixel on the digitized image $G_{white}(x,y)$ would be about the

average value of R_p. This was performed by utilizing an averaging function in *Image Lab* which digitized the number of images requested and the resulting image was the average of those images. The paper was moved while the software was digitizing. Next, an average grey level value was computed from the histogram of the white reference and subtracted by the dark frame value, avg($G_{white}(x,y)$)-G_{dark}. Finally,Eq. 4.4.2 was applied which involved the ratios of each pixel value of the image and the white reference multiplied by the average of the white reference.

Since the dark frame was already subtracted from the image after flat fielding, the following equation was used in place of eq. 4.4.1 for determining the relative reflectance for the image histogram.

$$R_{relative} = \frac{G_{flat}}{avg(G_{white}) - \min(G_{dark})} = \frac{R_{object}}{R_{paper}} \tag{4.4.3}$$

The next section explains the procedure used for measuring image microstructure data.

4.4.1 Procedure for measuring Image Microstructure Data from a Test Sample

(1) Select a test sample to be measured.

(2) Calibrate the instrumentation.

(a) Obtain the minimum dark frame gray level, $\min(G_{dark})$. The dark frame is the lens cap placed over the microscope's objective lens so no light enters the microscope.

(b) Obtain an averaged digitized image of a white frame, $G_{white}(x,y)$, by taking the average of eight images at different locations on the paper. To perform this use the averaging function in *Image Lab* and move the paper while the software is digitizing. Also, observe the histogram and make sure the histogram is not clipped and light intensity is high enough. Store white reference image in second image memory register in *Image Lab*.

(c) Obtain the average grey level from the histogram of the white frame, $\text{avg}(G_{white}(x,y))$.

(3) Select the darkest patch from the ink jet test sample.

(4) Digitize image of patch on test sample, $G(x,y)$.

(5) Flat field image by applying flat fielding program (written as an external program in *Image Lab*).

(6) Obtain histogram of flat fielded image, $G_{flat}(x,y)$, which is in *counts* vs. *grey level*.

(7) Convert *grey level* on histogram into $R_{relative}$ using eq. 4.4.3.

$$R_{relative} = \frac{G_{flat}}{avg(G_{white}) - \min(G_{dark})} = \frac{R_{object}}{R_{paper}} \tag{4.4.3}$$

(8) Obtain R, R_i , R_p, and F data from histogram as displayed in figure 4.4.1. Note, the reflectances are relative.

(9) Repeat steps 3 through 8 for the next eight to twelve lighter patches. (Number of patches measured depends on the amount that will display trend of data on plots)

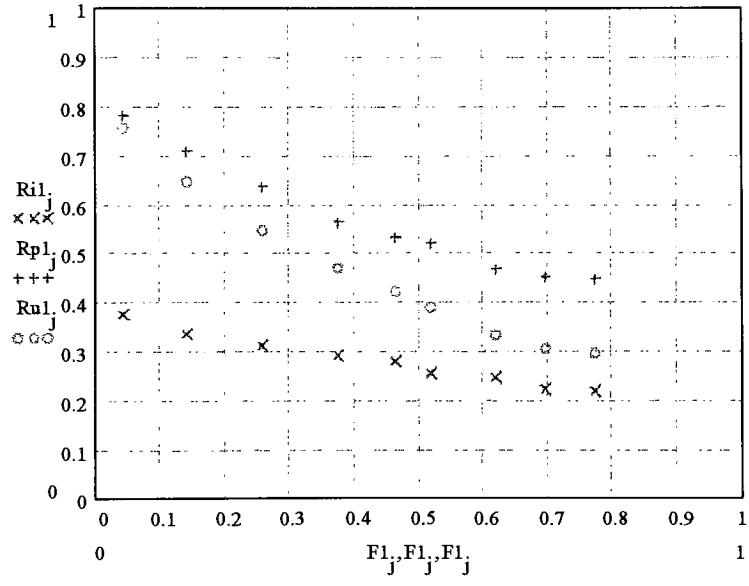

Figure 4.4.2: Sample of a plot of R, R_i , R_p, and F data obtained from nine patches on a test sample.

4.5 Technique for measuring a Line Scan on Halftone Dots

To measure a line scan of halftone dots on a test sample, the line scan function in *Image Lab* was utilized. By using the line scan function, a line is drawn across the region of interest on the image and three sets of data are produced which is the grey level, x-coordinate position, and y-coordinate position of a pixel along the line. The grey level was converted to optical density and the x and y coordinates were converted to distance so that the line scan plots were a function of *optical density* vs. *distance*. A program was written in *Mathcad* to perform the calculations and draw the plots of the line scans. The following explains the procedure for obtaining the line scan.

4.5.1 Procedure for Measuring the Line Scan on Halftone Dots

(1) Calibrate the instrumentation as in step 2 of section 4.4.1.

(2) Obtain the dimensions of the field of view of the digitized image.

(a) Place a ruler under the microscope in a diagonal position and digitize the image.

(b) Draw a line scan across the ruler. The line scan will give three sets of data: grey level, x-coordinate, and y-coordinate. The x and y coordinates are in pixel dimensions. The line scan will be sinusoidal with the lowest values representing the tick marks on the ruler.

(c) Obtain the angle of the line scan, θ, by taking the arctangent of the x(pixel) and y(pixel) coordinates. Obtain the following x and y values in millimeters through use of eq. 4.5.1 and eq. 4.5.2 with d (in millimeters) representing the distance measured on the ruler.

$$x(mm) = d\cos(\theta) \tag{4.5.1}$$

$$y(mm) = d\sin(\theta) \tag{4.5.2}$$

Since the resolution of a digitized image is 512 (x) by 464 (y) pixels, the dimensions of the field of view (fov) of the digitized image is obtained by eq. 4.5.3. and eq. 4.5.4.

$$x_{fov}(mm) = \frac{x(mm)}{x(pixel)} \cdot 512 \tag{4.5.3}$$

$$y_{fov}(mm) = \frac{y(mm)}{y(pixel)} \cdot 464 \tag{4.5.4}$$

$x_{fov}(mm)$ was measured 1.84 mm and $y_{fov}(mm)$ was measured 1.33 mm for the microdensitometry equipment used in this research.

---

(3) Select a test sample and a halftone pattern patch from the test sample for a line scan to be measured.

(4) Digitize image of patch on test sample, $G(x,y)$.

(5) Flat field image by applying flat fielding program (written as an external program in *Image Lab*).

(6) Obtain line scan of flat fielded image, $G_{flat}(x,y)$.

(7) Convert *grey level* on line scan into $R_{relative}$ using eq. 4.2.3.

$$R_{relative} = \frac{G_{flat}}{avg(G_{white}) - \min(G_{dark})} = \frac{R_{object}}{R_{paper}} \tag{4.2.3}$$

Convert $R_{relative}$ to R by multiplying by the paper's reflectance. Convert R to the optical density, D, through use of the following equation.

$$D = -\log(R) \tag{4.5.5}$$

(8) Convert the x and y pixel coordinates into distance (mm) by applying eq. 4.5.6, eq. 4.5.7, and eq. 4.5.8.

$$x(mm) = \frac{x(pixel) - x_o(pixel)}{512} \cdot x_{fov}(mm) \tag{4.5.6}$$

$$y(mm) = \frac{y(pixel) - y_o(pixel)}{464} \cdot y_{fov}(mm) \tag{4.5.7}$$

$$d(mm) = \sqrt{x(mm)^2 + y(mm)^2} \tag{4.5.8}$$

where, $x_o(pixel)$, $y_o(pixel)$: starting pixel coordinates of line scan.

4.6 Testing the Microdensitometry Equipment for Feasibility

The microdensitometry equipment was tested for its linearity by measuring the relative reflectances of a Kodak Gray Scale and comparing them to the relative reflectance measured by a densitometer. The reflectances were relative to the lightest patch on the gray scale. The following plot displayed the linearity of the microdensitometer

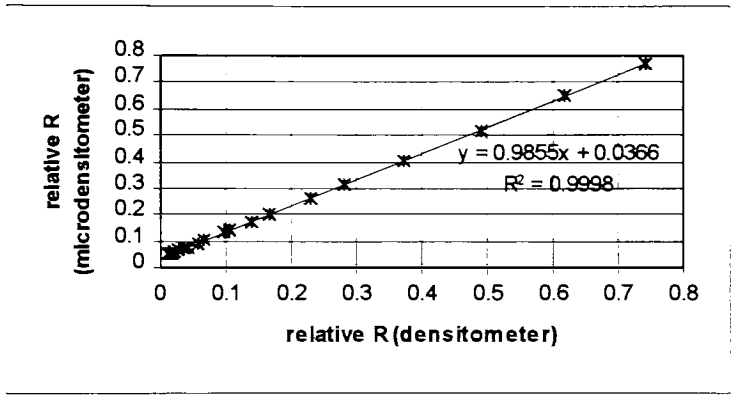

Figure 4.6.1: A plot displaying the linearity of the microdensitometer.

Before using the microdensitometer,the microdensitometer was tested for whether its MTF was feasible enough for measuring paper. A rule of thumb that was used for paper MTF was that the highest spatial frequency for paper was 10 cycles/mm. The MTF for the microdensitometer was measured using two techniques. One technique involved using a razor blade and another technique used a calibrated sinusoidal grating. The razor blade technique involved placing a razor blade under the microscope with light shining under the razor blade. This produced an image with one side black and the other

side white. A line scan was taken across the image which produced a step function. The derivative of the step function produced a line spread function. The Fourier Transform of the line spread function produced the MTF of the system. The sinusoidal grating consisted of several patterns of transmittance varying sinusoids at different known spatial frequencies. The MTF was measured from the amplitudes of the sine waves. Plots of the microdensitometer's MTF for both techniques is displayed in figures 4.6.2 and 4.6.3 which demonstrated that the microdensitmeter's MTF was larger than paper's MTF since both provided a frequency of 40 cycles/mm at 50% threshold.

The microdensitometer was also tested for repeatability of its reflectance measurements. A test sample with a printed halftone pattern was used as a reference that produced a nicely shaped histogram. Histograms were measured consecutively and analyzed for any changes. The following plots in figure 4.6.4 displayed the repeatability of the microdensitometer.

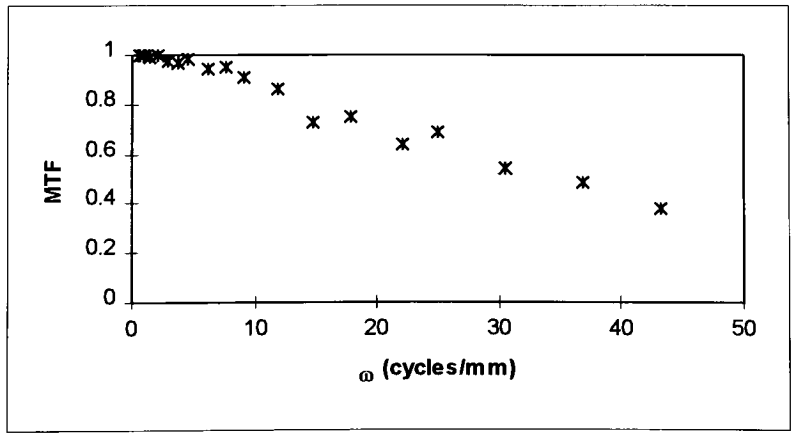

Figure 4.6.2: MTF of microdensitometer measured using razor blade technique.

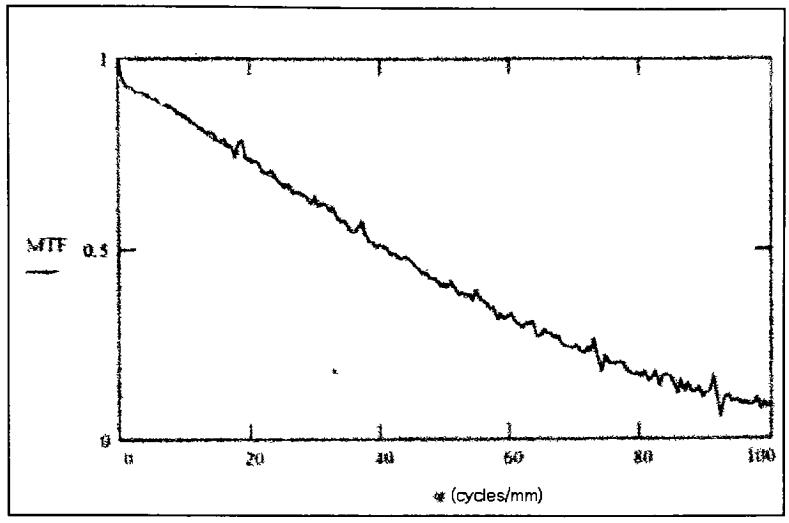

Figure 4.6.3: MTF of microdensitometer measured using sinusoidal grating technique.

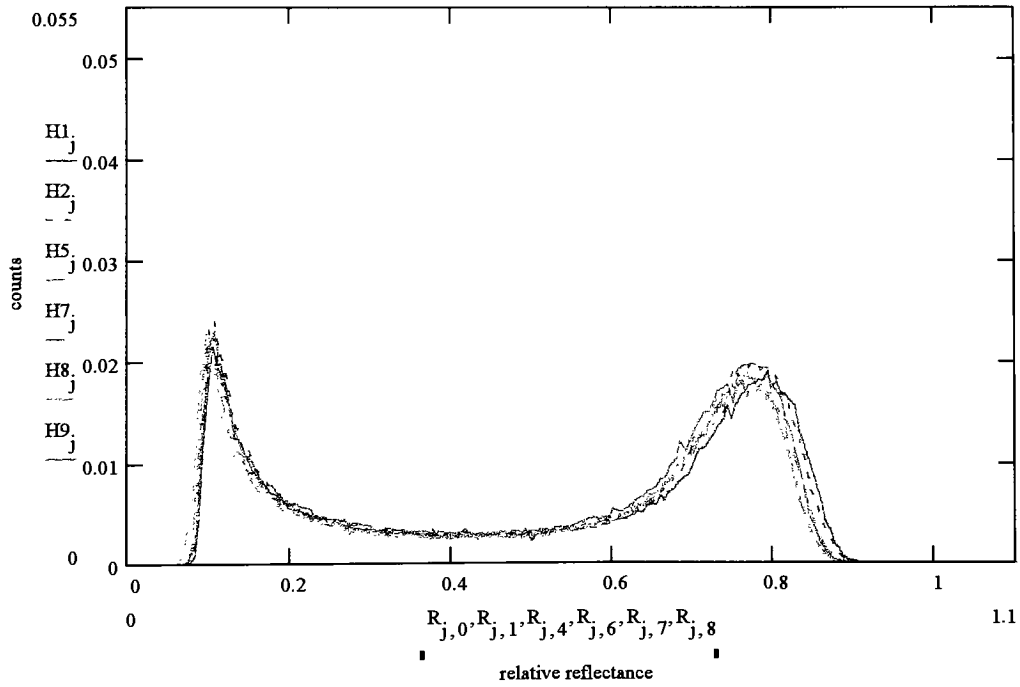

Figure 4.6.4: The microdensitometer was test for repeatability by obtaining six consecutively measured histograms of a reference halftone pattern.

4.7 Determining the empirical F vs. F_o equation

Before determining an empirical F vs. F_o equation, values for F_o needed to be measured. The HP1600C used a gray level, G, to print a tone. The ideal dot area fraction F_o and G were estimated to be linearly related and the following equation was designed.

$$F_o = 1 - \frac{G}{255} \tag{4.7.1}$$

The succeeding power function was designed to relate F_o to the measured F for the HP1600C printer.

$$F = F_o^{1/m} F_r \tag{4.7.2}$$

For the ENCAD printer, instead of using a gray level the ENCAD samples supplied an ideal dot area fraction as shown on the sample in figure 4.1.1 (b). This supplied dot area fraction was given the variable name G. It was observed that the relationship between G and F_o took on a Yule-Nielson type of relationship so it was assumed that the printer had a Yule-Nielson algorithm. Thus, the following equation was used to undo the Yule-Nielson algorithm.

$$F_o = 1 - (1 - G)^{1/n} \tag{4.7.3}$$

After observing the data for F_o and F, it was noticed the relationship was linear. The next equation was used to relate F_o to F for the ENCAD printer.

$$F = F_o F_r \tag{4.7.4}$$

4.7.1 Procedure for applying the Empirical F vs. F_o equations and F_o equations for the HP1600C printer and ENCAD printer

HP1600C	ENCAD
Procedure	Procedure
(1) Obtain F (measured dot area fraction) and G data. G: grey level (0 to 255)	(1) Obtain F (measured dot area fraction) and G data. G: dot area fraction command sent to printer (0% to 100%)
(2) Apply eq. 4.7.1 to obtain F_o. $F_o = 1 - \frac{G}{255}$ (4.7.1)	(2) Apply eq. 4.7.3 to obtain F_o. $F_o = 1 - (1-G)^{1/n}$ (4.7.3)
(3) Apply the F vs. F_o equation (eq. 4.7.2) to the data. Adjust values for m an d F_r until the equation fits the data. $F = F_o^{1/m} F_r$ (4.7.2) m, F_r: calibration parameters	(3)Apply the F vs. F_o equation (eq. 4.7.4) to the data. Adjust values for n an d F_r until the equation fits the data. $F = F_o F_r$ (4.7.4) n, F_r: calibration parameters

The procedures described above were fitted to the data by adjusting the calibration parameters until the root mean squared error (RMS) was at its lowest value. A program written in *MATHCAD* was used in applying the empirical equations to the data. The next equation is the equation for the root mean squared error.

$$RMS_{dot} = \sqrt{\sum_{j} \frac{\left(Fdata_j - F\bmod el(G_j)\right)^2}{N}} \qquad (4.7.5)$$

where, *Fdata*: measured dot area fraction from data

Fmodel(G_j): dot area fraction calculated from empirical equation as a function of G

N: number of patches on test sample measured

Note: *Fmodel*(G_j) *is a* functions of G as opposed to F because F is a function of F_o and F_o is a function of G.

Figure 4.7.1 displays the empirical equations fitted to the data for the HP1600C and figure 4.7.2 displays the equations fitted for the ENCAD printer. Plots for all the test samples are displayed in appendix A.

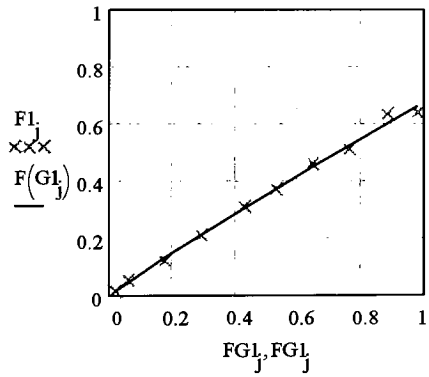

(a) sample 1
$F_r = 0.676$ m = 1.061
RMS_{dot}=0.0147

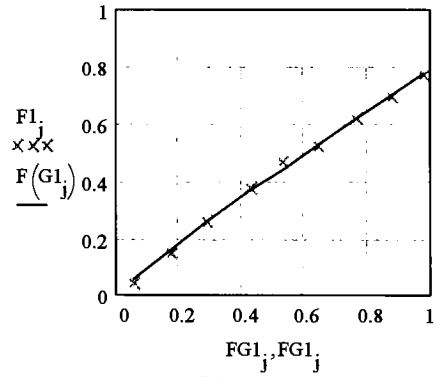

(b) sample 2
$F_r = 0.789$m = 1.089
RMS_{dot}=0.0123

Figure 4.7.1: Empirical F vs. F_o equations applied to the data for the HP1600C printer.

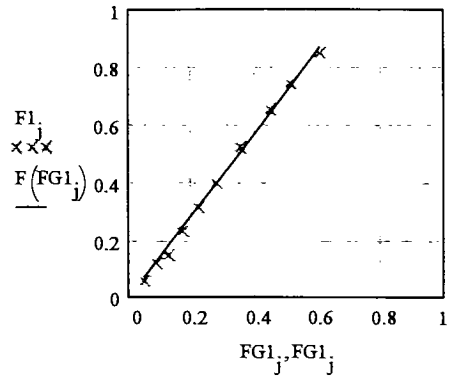

(a) sample 14
$F_r = 1.42$ m = 3.181
RMS_{dot}=0.01557

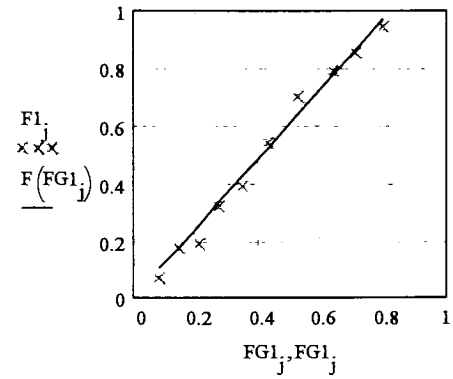

(b) sample 16
$F_r = 1.214$ m = 1.865
RMS_{dot}=0.03503

Figure 4.7.2: Empirical F vs. F_o equations applied to the data for the ENCAD printer.

4.8 Applying the Modified Probability Model

After calibrating the F vs. F_o equation for a test sample, the equations in the Modified Probability Model were applied to the R vs. F, R_i vs. F, and R_P vs. F data by following the procedure in section 3.9.3. This was performed by writing a program in MATHCAD that plotted the data and also the Modified Probability Model. Because the data collected for R, R_i, and R_p were normalized to R_g, the data was multiplied by the measured value of R_g of the paper (obtained from table 4.1.2).

The halftone geometry utilized in the test samples was a dispersed dot halftone pattern. The equation for P_{po} (eq. 3.9.27) depended on the type of halftone geometry used and the equation that was chosen from table 3.8.1 was the following.

$$P_{po}=w(1-(1-F)^B) \tag{3.9.27}$$

From table 3.8.1, the parameter B for a stochastic halftone geometry was a value of 1.2. As will be discussed in section 5.0, B was set at 1.2 for the ENCAD printer and 2.0 for the HP1600C.

To have the model achieve the best fit to the data, w, Sx, and ε were used to adjust the model until the root mean squared error between the data point's value and the model's value was at its lowest value. A program written in *MATHCAD* was used in applying the model to the data. The root mean squared error used was calculated from the following equation .

$$RMS_{tot} = \sqrt{\sum_j \frac{\left(Ridata_j - Ri\bmod el(G_j)\right)^2 + \left(Rpdata_j - Rp\bmod el\ (G_j)\right)^2}{2N}} \quad (4.8.1)$$

where, $Ridata_j$, $Rpdata_j$: measured reflectances from data

$Rimodel(G_j)$, $Rpmodel(G_j)$: calculated reflectances from the Modified Probability Model as a function of G

N: number of patches on test sample measured

Note: $Rimodel(G_j)$, $Rpmodel(G_j)$ are functions of G as opposed to F because F is a function of F_o and F_o is a function of G.

Figure 4.8.1 displays the Modified Probability Model fitted to the data with the parameters ε, w, and Sx set at the following values. Plots of all the test samples of which

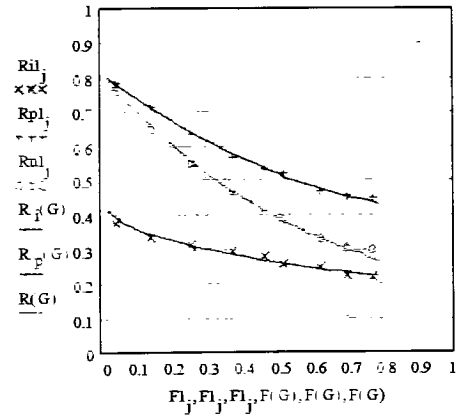

sample 2

ε=0.0578 w=0.70961 Sx=0.711 RMS_{tot}=0.00844

Figure 4.8.1: Sample of data of which the Modified Probability Model was fit to.

After completing a best fit for each test sample, the model was judged on how well its R vs. F, R_i vs. F, and R_P vs. F curves fitted the data. If the curves were determined to fit the data well, then the Modified Probability Model will be considered as being suitable enough for modeling tone reproduction curves by considering ink spread and ink penetration .

Next, the properties of the parameters Sx and ε were analyzed by studying the independent effects of the various printing conditions (paper, ink, heat, two color overprint, and etc.) would have on them. Sx is related to the light scattering and penetration properties of the ink and ε is related to the absorption properties of the ink. These parameters would provide a key quantitative measure of the inherent properties of ink caused by printing conditions through use of image microstructure data.

5. *Results*

As was discussed in section 4.8, the equation for P_{po} (eq. 3.9.27) was dependent on the type of halftone geometry and was chosen from table 3.8.1. The type of halftone geometry utilized was a disperse dot halftone and the equation chosen from the table was the following.

$$P_{po}=w(1-(1-F)^{B}) \tag{3.9.27}$$

From table 3.8.1, B set at 1.2 would represent a stochastic halftone geometry. For all the test samples for the ENCAD printer, B set at 1.2 fitted the data well. For the test samples for the HP1600C, a better fit was achieved when B was set at 2.0 (which was the

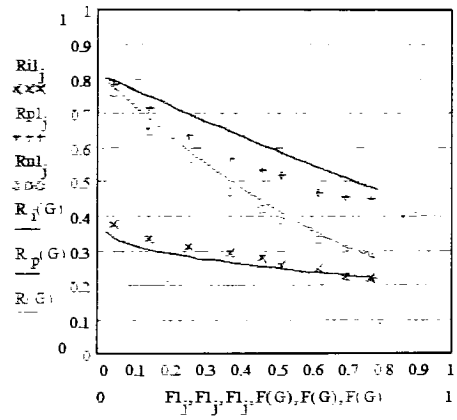

sample 2
ε=0.0578 w=0.710 Sx=0.711
RMS=0.04582
(a) B=1.2

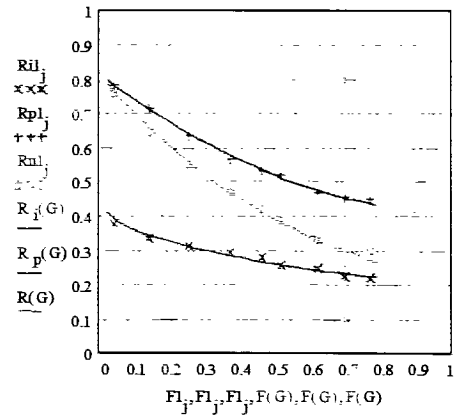

sample 2
ε=0.0578 w=0.710 Sx=0.711
RMS=0.00844
(b) B=2.0

Figure 5.1: For the HP1600C, the parameter B set at 2.0 fitted the data better.

value for the FM spaces geometry) as displayed in figure 5.1. B set at 2.0 provided a curvature to the R_p vs. F curve of which the data resembled. B set at 1.2 made the curve more linear. Therefore, B was set at a value of 2.0 for all the test samples for the HP1600C. The value of 2.0 for B maybe justifiable since the value for B from table 3.8.1 were determined empirically from a stochastic pattern produced by a different printing process and was not tested on the halftone geometry the HP1600C printer produced.

As mentioned, all the plots of which the model was fitted to are displayed in appendix A. For most of the plots, the model fitted the data very well. The test sample

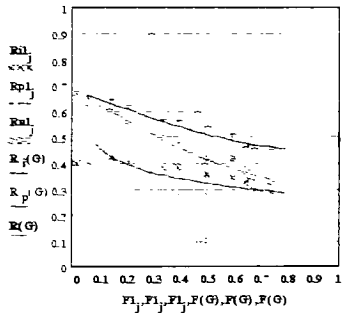

(a) sample 3

ε=0.2023 w=0.489 Sx=4.844

RMS=0.03191

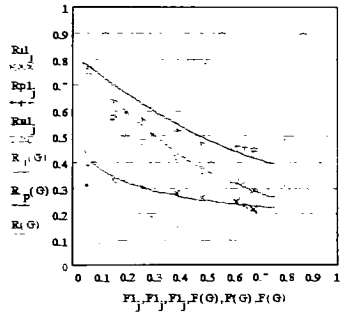

(b) sample 6

ε=0.0897 w=0.538 Sx=0.869

RMS=0.02340

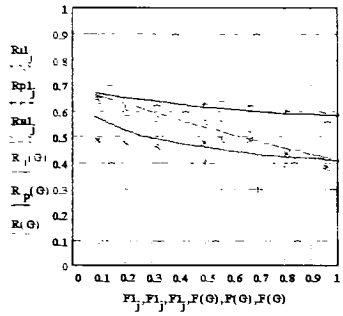

(c) sample 17

ε=0.1555 w=0.244 Sx=3.706

RMS=0.01881

Figure 5.2: Test samples of which the data was the most difficult for the Modified Probability Model to fit.

of which the model fitted the best was sample 2 (figure 5.1b) with an RMS equal to 0.00844 and the worst fit was sample 3 (figure 5.2a) with an RMS value of 0.03191. The next worst fit was sample 6 (figure 5.2b) with an RMS value of 0.02340 and then sample 7 (figure 5.2c) with an RMS value of 0.01881.

The accuracy of the data from test sample 3 is questionable. The pattern of the data for the ink reflectance did not appear to follow the same general pattern of other test patterns. Another test sample produced would have confirmed if the data was correct. The accuracy of the data for the two color overprint test samples (samples 17 and 19) are also questionable. Data was very difficult to measure from these test samples since the halftone dots were very distorted and washed out. The difference in values for ε, w, and Sx for test samples 3, 17, and 19 compared to other test samples was large.

Next, what will be discussed is the effect the printing conditions had on the parameters Sx and ε. Sx and ε were related to the inherent properties of the ink with Sx related to the light scattering and penetration properties and ε related to the light absorption efficiency. The printing conditions were analyzed by grouping test samples with the same printing conditions except with one of the printing conditions varied. The effect a printing condition had on the Sx or ε parameter was analyzed by plotting the value of Sx or ε for one printing condition and plotting the value of Sx or ε for the other

printing condition. The test sample number was labeled next to the data point. The printing conditions that were analyzed were *uncoated paper* vs. *synthetic paper*, *no surfactant* vs. *surfactant* added to the ink, *pigmented ink* vs. *dyed ink*, *no heat* vs. *heat* applied, and *single color print* vs. *two color overprint*.

For uncoated paper vs. synthetic paper, it was expected that ink penetration would increase and therefore the *Sx* value would increase. Figure 5.3 (a) displayed that generally most of the *Sx* values (6 out of 9 data sets) for uncoated paper were larger. Figure 5.3 (b) displayed the effect uncoated paper and synthetic paper had on ε. It was observed that 6 of the 9 data set values had a larger value for ε for synthetic paper. This could have indicated that uncoated paper decreased the absorption efficiency of the ink. When the ink penetrated into the paper, the halftone dot consisted of both the ink and the paper. Since the absorption strength of paper is lower than the absorption strength of

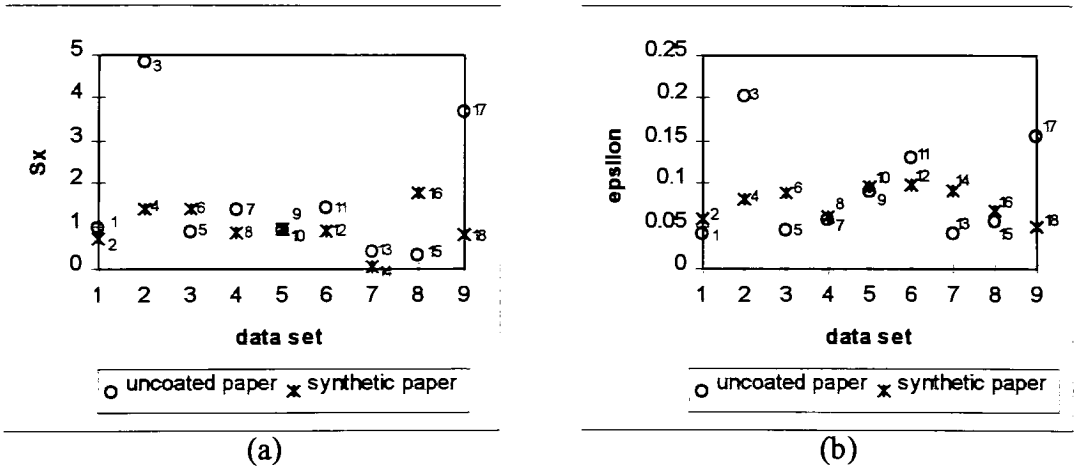

(a) (b)

Figure 5.3: The effect of *uncoated paper* vs. *synthetic paper* on *Sx* and ε.

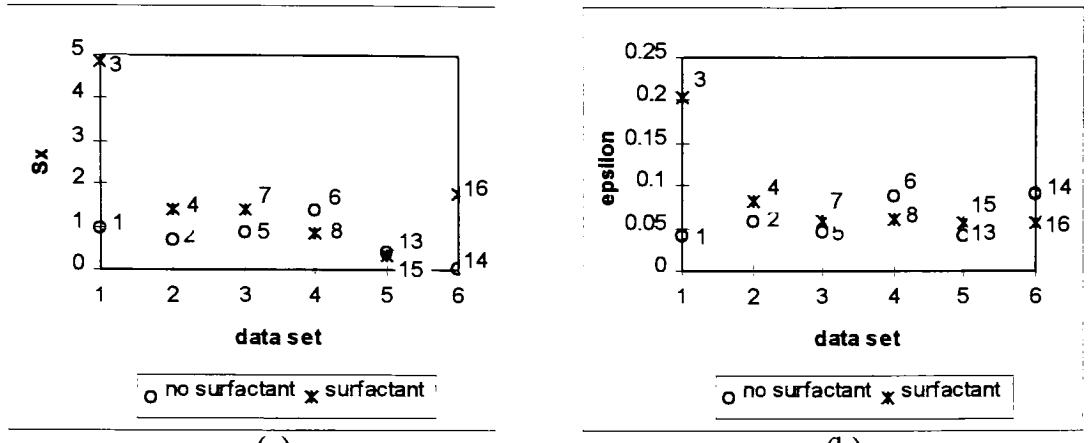

(a) (b)

Figure 5.4: The effect of ink with *no surfactant* vs. ink with *surfactant* on *Sx* and ε.

ink, the absorption strength of the halftone dot could have decreased.

For ink with no surfactant vs. ink with surfactant, 4 of the 6 data sets in figure 5.4 (a) displayed that ink with surfactant had *Sx* values that were larger. This may have indicated that surfactant added to the ink may have caused the ink to penetrate into the paper more. In figure 5.4 (b), 4 of the 6 data sets indicated that ε increased as surfactant was added to the ink. The absorption efficiency might have increased due to surfactant added to the ink. Surfactant was intended to cause the ink to spread more. If the ink spread more, the particles of the colorant would be more spread out. This could have increased the absorption strength of the colorant particles since the individual colorant particles would have had a better chance of being struck by a photon.

Figure 5.5 (a) displayed the effect pigmented ink and dyed ink had on the *Sx*

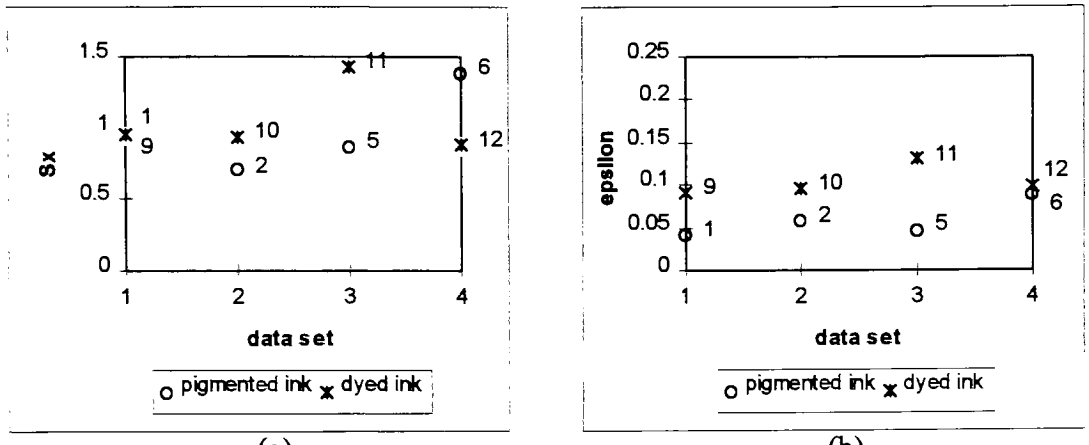

(a) (b)

Figure 5.5: The effect of *pigmented ink* vs. *dyed ink* on *Sx* and ε.

value. It was expected that dyed ink would have a larger *Sx* value. Dyed ink was expected to penetrate into the paper more than pigmented ink since dye particles are smaller than pigment particles but only 2 of the 4 data sets had a larger *Sx* value for dyed ink. For the ε value, 4 out of the 4 data sets for dyed ink had a larger ε value as shown in figure 5.5 (b). This coincided with the expectation that dyed ink had a higher absorption strength than pigmented ink.

For no heat vs. heat applied, figure 5.6 (a) displayed that for half of the data the *Sx* value decreased when heat was applied. Since only half of the data was affected by heat, heat may have not have had much of an effect on the *Sx* parameter or not enough heat was applied to have an effect. *Sx* was expected to decrease when heat was applied since it was expected that ink penetration would be reduced by heat. Figure 5.6 (b) displayed the effect the application of heat had on the ε parameter. Again, it was

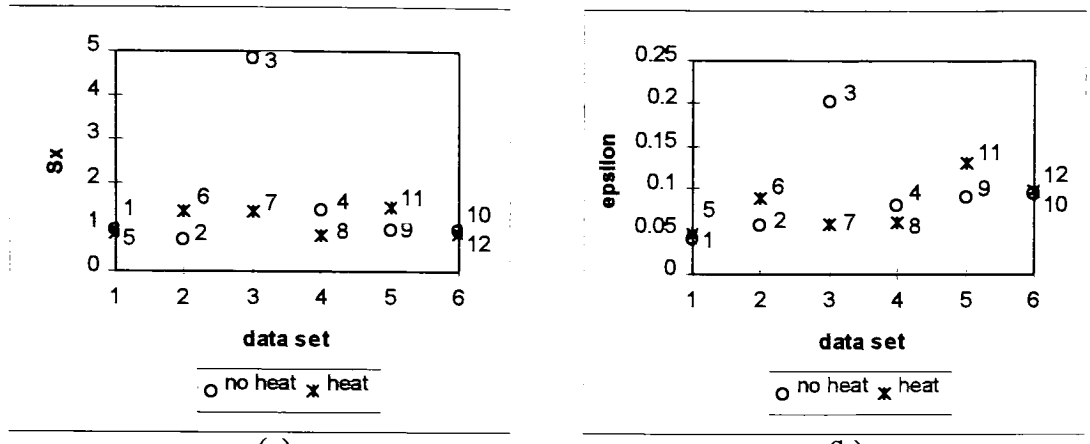

(a) (b)

Figure 5.6: The effect of *no heat* applied vs. *heat* applied on *Sx* and ε.

difficult to determine if heat had an effect on ε since the value of ε was not biased toward any printing condition (meaning ε was not consistently larger for one of the printing conditions).

For the last printing condition, single color print vs. two color overprint, the data indicated that *Sx* was generally not affected by a two color overprint. It was expected

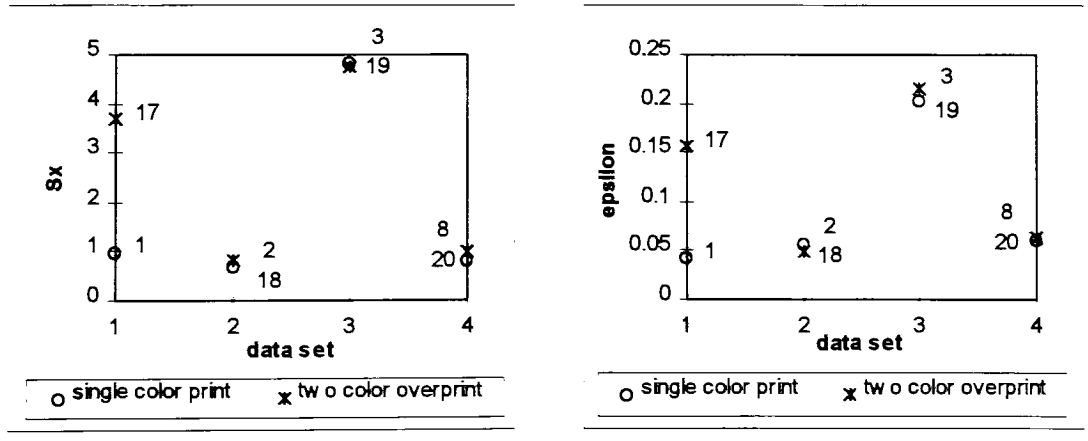

(a) (b)

Figure 5.7: The effect of *single color print* vs. *two color overprint* on *Sx* and ε.

that Sx would be higher due to a two color overprint. A two color overprint made the paper more wet. A more wet paper was thought was thought to make the paper wick the ink even more which would increase ink penetration. The value for ε also generally did not seem to be affected by a two color overprint as shown in figure 5.7 (b). It was thought that ε would increase in value due to a two color overprint. A two color overprint caused the ink to spread more. Since the ink would spread more, the absorption efficiency of the colorant particle would increase due to the increased probability of being struck by a photon.

6. Conclusions and Recommendations

The Modified Probability Model was tested for its ability to model tone reproduction on data that was measured from test samples under different printing conditions that affected ink penetration, ink spread, and simulated other ink jet environments. From the data obtained, it was found that the model fitted the data generally very well. There were some questionable peculiarities that occurred. One peculiarity was the B parameter for the P_{po} equation (eq. 3.9.27). The halftone geometry used in this study was a stochastic halftone pattern and the B parameter from a past study was determined empirically to be a value of 1.2 (from table 3.8.1). This value worked well for the ENCAD printer. For the HP1600C printer, it was determined that a value of 2.0 worked better even though this value was related to an FM spaces halftone geometry. Since the value for the B parameter was determined empirically from a stochastic geometry produced by a printing process that was different from the HP1600C printer, a value of 2.0 could be considered valid for the HP1600C printer.

Other peculiarities was that there were some tone reproduction data from test samples of which the model did not fit well. This may have been due to the production of the test samples, the measurement of the data, or some factors that may have not been considered in the model.

The parameters of the model that were related to some inherent properties of ink were analyzed on how printing conditions would affect them. The Sx parameter was

related to the light scattering and the degree of penetration into paper of the ink and ε was related to the absorption strength of the ink. Uncoated paper and synthetic paper was used to control ink penetration The *Sx* parameter was greater in value for most of the data analyzed for uncoated paper. Dyed ink has a higher absorption strength than pigmented ink. For the ε parameter, all of the values that were analyzed for ε were greater for dyed ink than pigmented ink. Other printing conditions did not have much of a biased effect on *Sx* and ε. For heat applied and not applied to the paper, it was expected that heat would decrease ink penetration. The *Sx* parameter did not clearly indicate this. What may have occurred was that ink penetration may have not been affected enough to be detected by the *Sx* parameter.

To quantitatively study the effect ink penetration has on the *Sx* parameter, what is suggested is to produced test patterns of ink on different substrates with calibrated absorption rates and to compare the absorption rates to the values of *Sx*. Also, to quantitatively study the effect the absorption strength of the ink has on the ε parameter, it is suggested to produce test samples with calibrated inks with different light absorption strengths and to compare the known values of ε with values of ε obtained from the model.

Other studies on the model that could be performed is to study the effect of a 3 and a 4 color overprint would have on the model. Another study could involve studying

the effect toner from a laser printer has on the model.

The Modified Probability Model did provide to be a sound model at producing the tone reproduction curves for image microstructure data collected in this study. It provides to be a strong analytical tool as compared to other tone reproduction models since its parameters are linked to physical and optical characteristics of ink-paper systems.

Appendix. Tone Reproduction Plots

Sample 1: ink= pigmented without surfactant paper= uncoated
heat= not applied printer= HP1600C

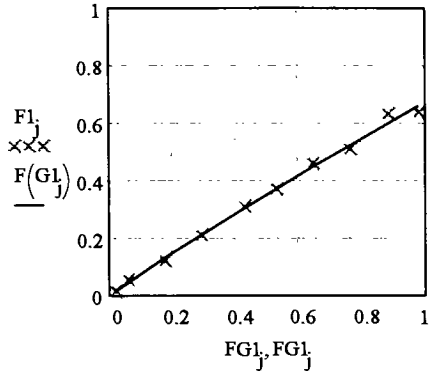

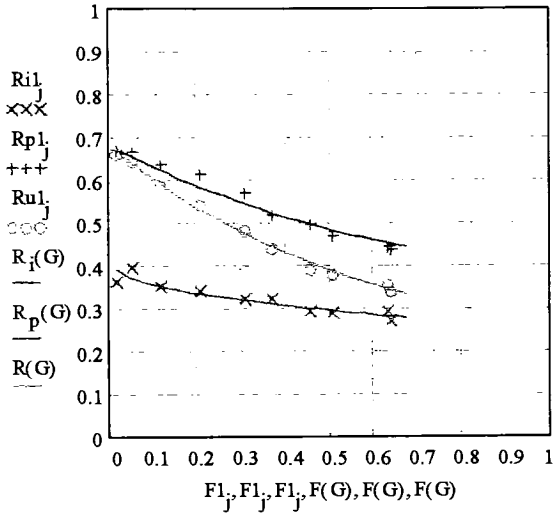

F_r=0.676 m=1.061 c=7.31 R_g=0.68 ε=0.431 w=0.607 B=2 Sx=0.959
RMS_{dot}=0.0147 RMS_{tot}=0.01483

Sample 2: ink= pigmented without surfactant paper= synthetic
heat= not applied printer= HP1600C

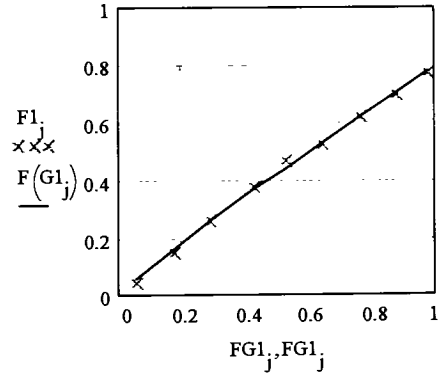

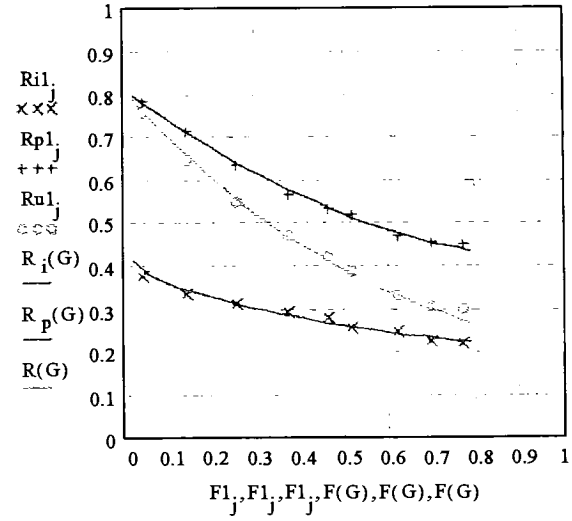

F_r=0.789 m=1.089 c=7.31 R_g=0.81 ε=0.0578 w=0.710 B=2 Sx=0.711
RMS_{dot}=0.0123 RMS_{tot}=0.00844

Appendix. Tone Reproduction Plots

Sample 3: ink= pigmented with surfactant paper= uncoated
heat= not applied printer= HP1600C

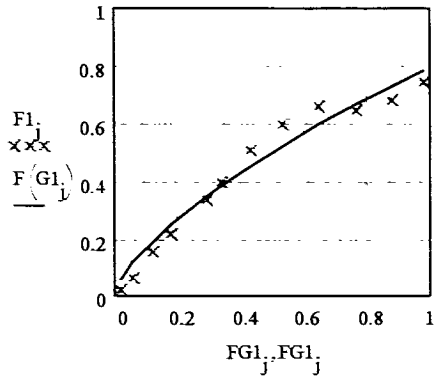

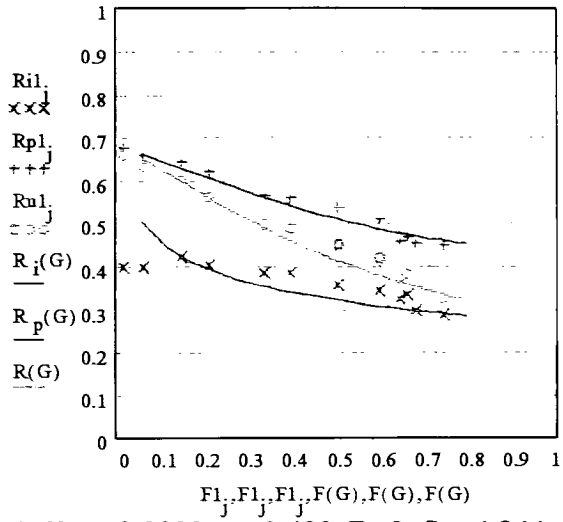

F_r=0.796 m=1.487 c=7.47 R_g=0.68 ε=0.2023 w=0.489 B=2 Sx=4.844
RMS_{dot}=0.0464 RMS_{tot}=0.03191

Sample 4: ink= pigmented with surfactant paper= synthetic
heat= not applied printer= HP1600C

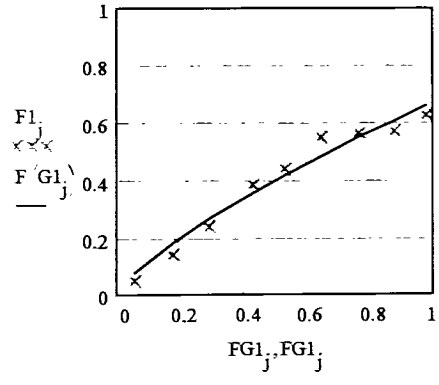

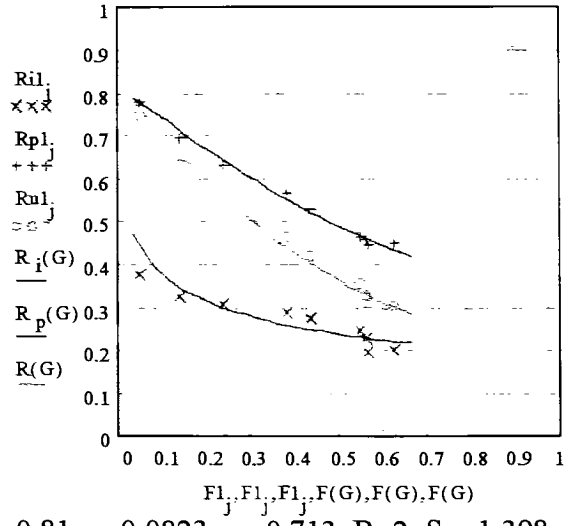

F_r=0.667 m=1.33 c=7.47 R_g=0.81 ε=0.0823 w=0.713 B=2 Sx=1.398
RMS_{dot}=0.03671 RMS_{tot}=0.01758

Appendix. Tone Reproduction Plots

Sample 5: ink= pigmented without surfactant paper= uncoated
heat= applied printer= HP1600C

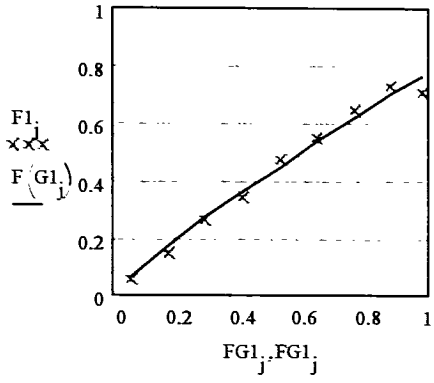

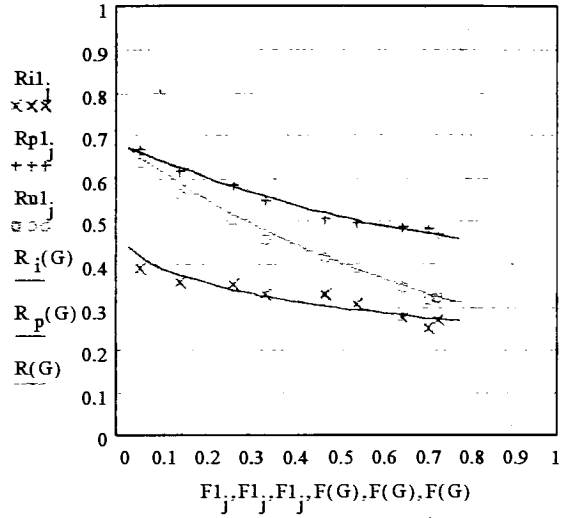

F_r=0.78 m=1.145 c=7.31 R_g=0.68 ε=0.0476 w=0.538 B=2 Sx=0.869
RMS_{dot}=0.02856 RMS_{tot}=0.01191

Sample 6: ink= pigmented without surfactant paper= synthetic
heat= applied printer= HP1600C

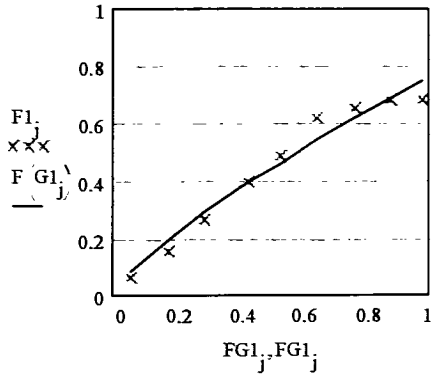

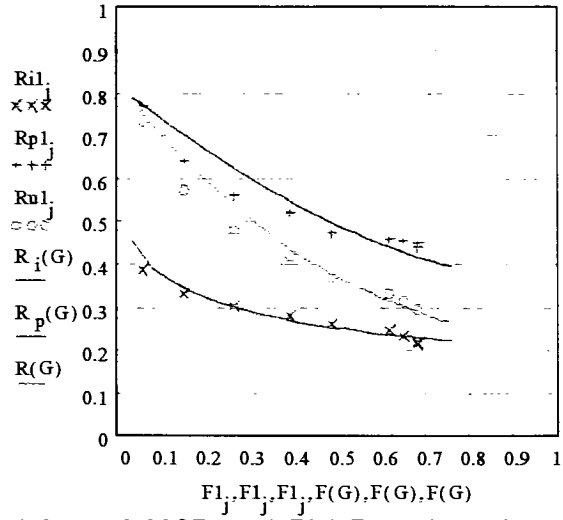

F_r=0.759 m=1.278 c=7.31 R_g=0.81 ε=0.0897 w=0.726 B=2 Sx=1.381
RMS_{dot}=0.04129 RMS_{tot}=0.0234

Appendix. Tone Reproduction Plots

Sample 7: ink= pigmented with surfactant paper= uncoated
heat= applied printer= HP1600C

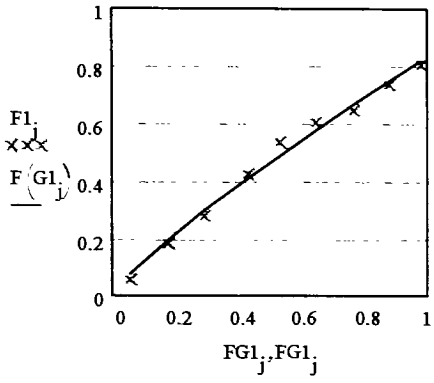

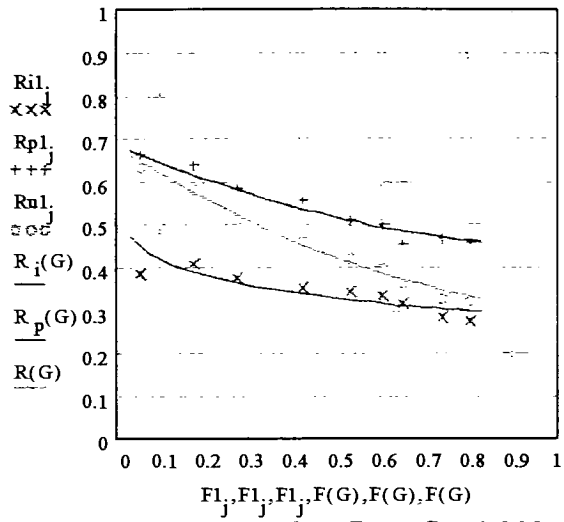

F_r=0.83 m=1.199 c=7.47 R_g=0.68 ε=0.0589 w=0.521 B=2 Sx=1.382
RMS_{dot}=0.02264 RMS_{tot}=0.01927

Sample 8: ink= pigmented with surfactant paper= synthetic
heat= applied printer= HP1600C

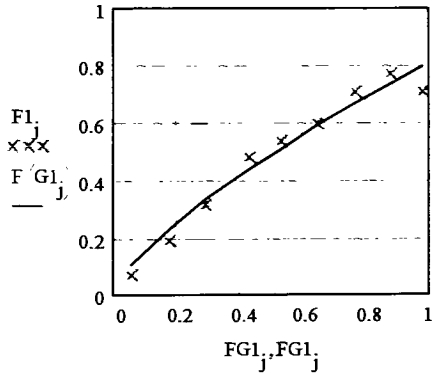

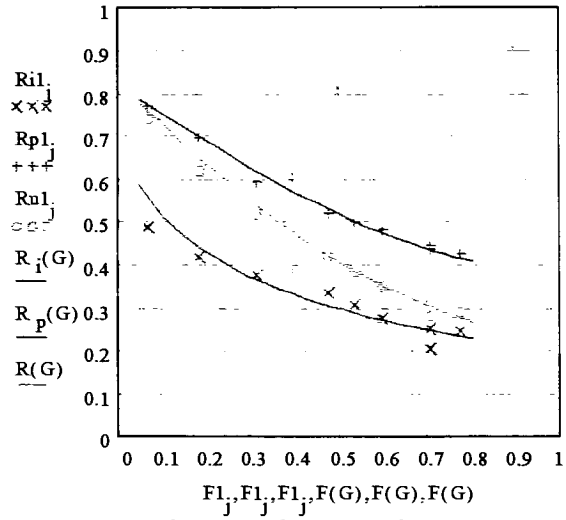

F_r=0.808 m=1.377 c=7.47 R_g=0.81 ε=0.06 w=0.750 B=2 Sx=0.820
RMS_{dot}=0.04333 RMS_{tot}=0.0165

Appendix. Tone Reproduction Plots

Sample 9: ink= dyed without surfactant paper= uncoated
heat= not applied printer= HP1600C

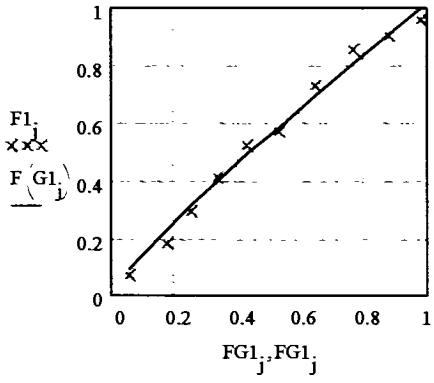

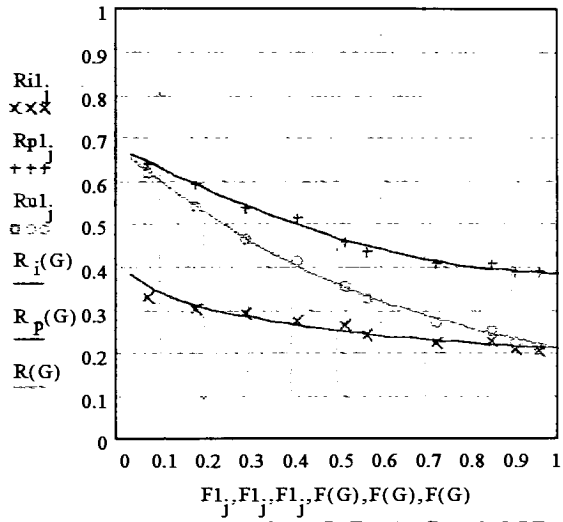

F_r=1.017 m=1.154 c=7.14 R_g=0.68 ε=0.0914 w=0.605 B=2 Sx=0.957
RMS_{dot}=0.02998 RMS_{tot}=0.00964

Sample 10: ink= dyed without surfactant paper= synthetic
heat= not applied printer= HP1600C

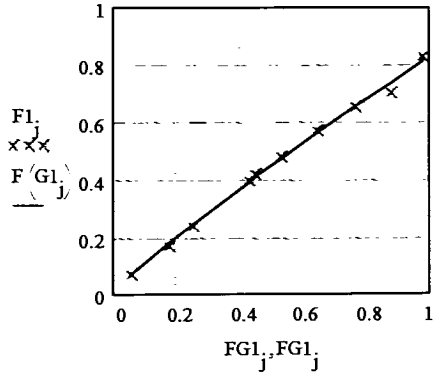

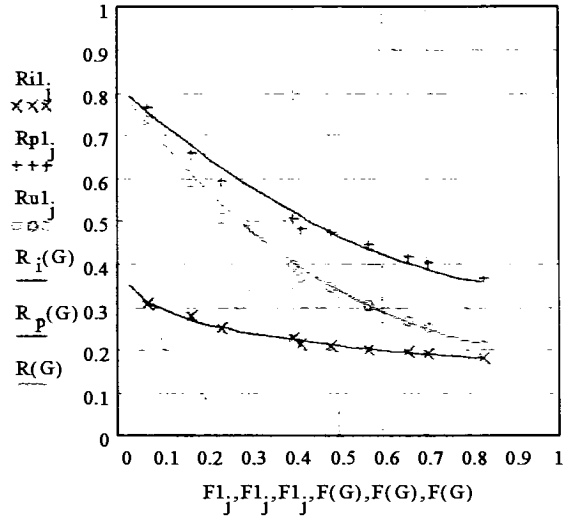

F_r=0.824 m=1.132 c=7.14 R_g=0.81 ε=0.0949 w=0.748 B=2 Sx=0.942
RMS_{dot}=0.01458 RMS_{tot}=0.01266

Appendix. Tone Reproduction Plots

Sample 11: ink= dyed without surfactant paper= uncoated
heat= applied printer= HP1600C

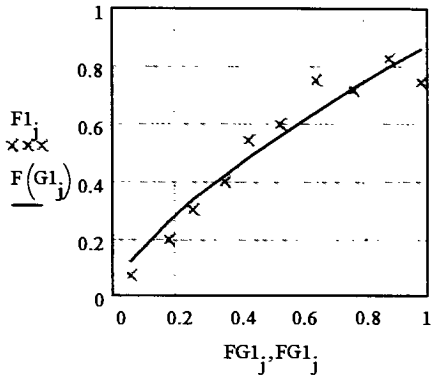

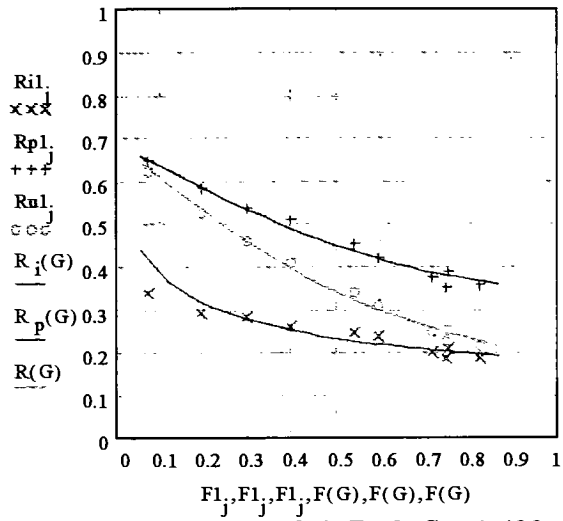

F_r=0.872 m=1.416 c=7.14 R_g=0.68 ε=0.1315 w=0.610 B=2 Sx=1.433
RMS_{dot}=0.06206 RMS_{tot}=0.01613

Sample 12: ink= dyed without surfactant paper= synthetic
heat= applied printer= HP1600C

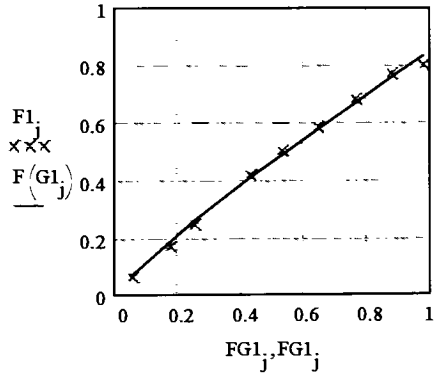

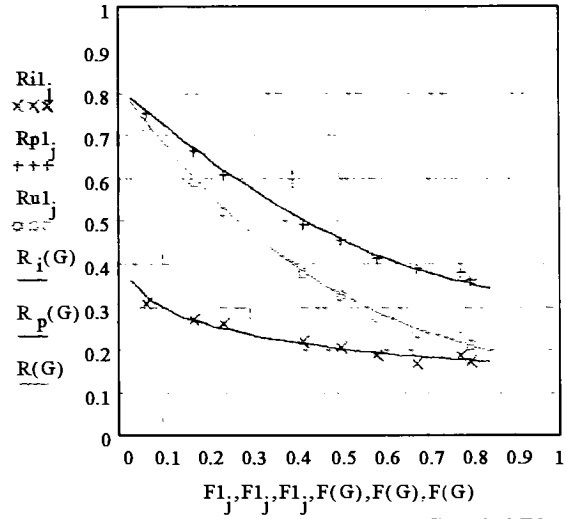

F_r=0.844 m=1.151 c=7.14 R_g=0.81 ε=0.0989 w=0.755 B=2 Sx=0.879
RMS_{dot}=0.01737 RMS_{tot}=0.01054

Appendix. Tone Reproduction Plots

Sample 13: ink= pigmented without surfactant paper= uncoated
heat= unknown printer= ENCAD

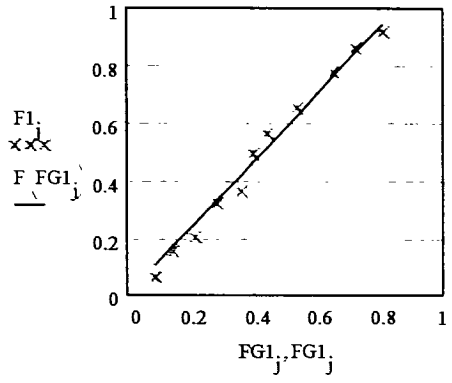

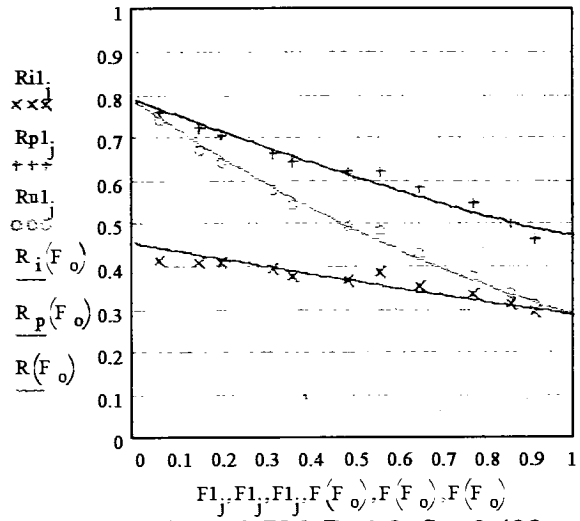

F_r=1.169 n=1.798 c=7 4 R_g=0.79 ε=0.0413 w=0.786 B=1.2 Sx=0.432
RMS_{dot}=0.03337 RMS_{tot}=0.00985

Sample 14: ink= pigmented without surfactant paper= synthetic
heat= unknown printer= ENCAD

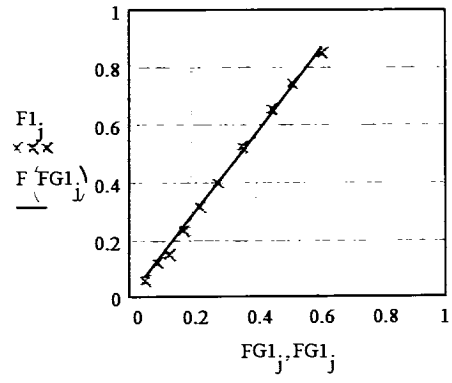

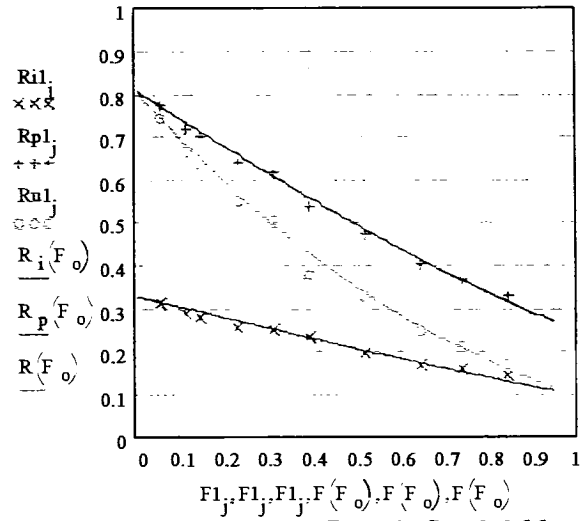

F_r=1.42 n=3.181 c=7.4 R_g=0.81 ε=0.0908 w=1.000 B=1.2 Sx=0.066
RMS_{dot}=0.01557 RMS_{tot}=0.01384

Appendix. Tone Reproduction Plots

Sample 15: ink= pigmented with surfactant paper= uncoated
heat= unknown printer= ENCAD

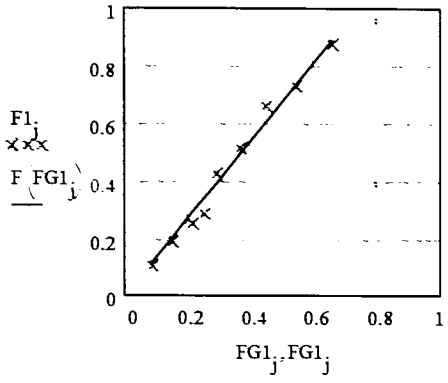

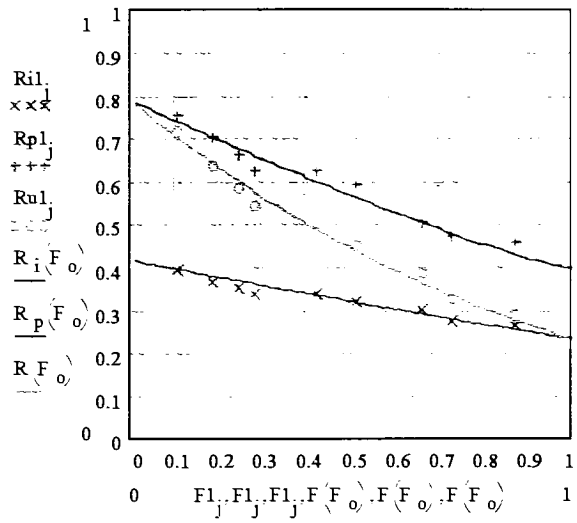

F_r=1.347 n=1.753 c=7.4 R_g=0.79 ε=0.057 w=0.875 B=1.2 Sx=0.318
RMS_{dot}=0.0343 RMS_{tot}=0.01186

Sample 16: ink= pigmented with surfactant paper= synthetic
heat= unknown printer= ENCAD

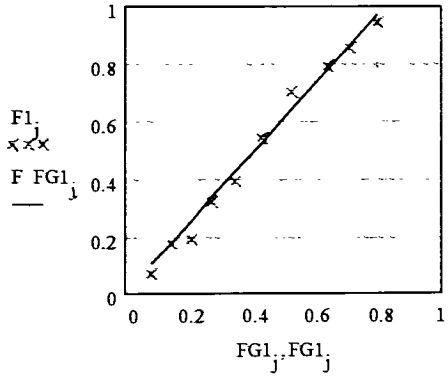

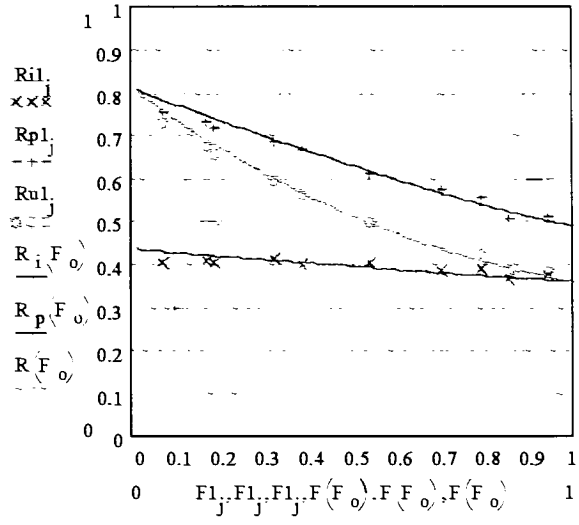

F_r=1.214 n=1.865 c=7.4 R_g=0.81 ε=0.0677 w=0.698 B=1.2 Sx=1.769
RMS_{dot}=0.03503 RMS_{tot}=0.00972

Appendix. Tone Reproduction Plots

Sample 17: ink= pigmented w/o surf. on top of dyed paper= uncoated
heat= not applied printer= HP1600C

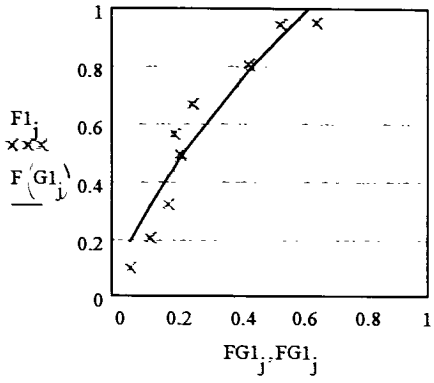

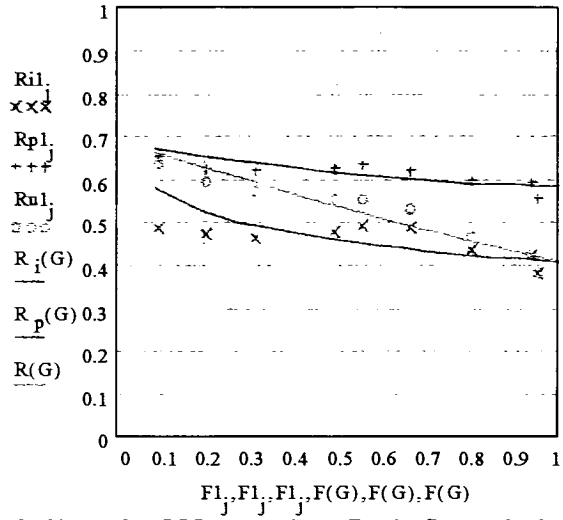

F_r=1.423 m=1.403 c=7.31 R_g=0.68 ε=0.1555 w=0.244 B=2 Sx=3.706
RMS_{dot}=0.08787 RMS_{tot}=0.01881

Sample 18: ink= pigmented w/o surf. on top of dyed paper= synthetic
heat= not applied printer= HP1600C

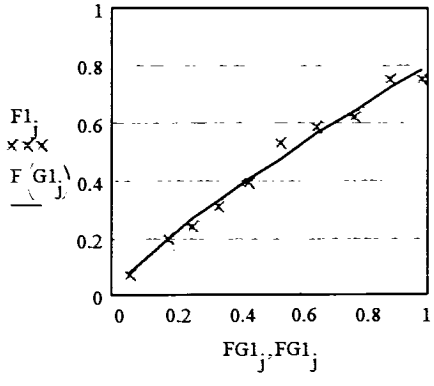

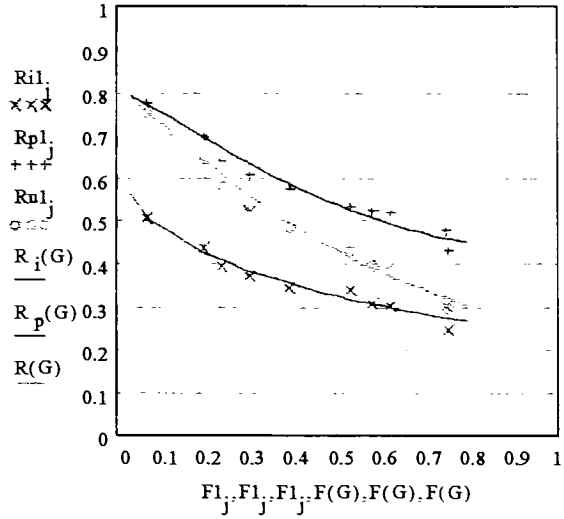

F_r=0.799 m=1.222 c=7.31 R_g=0.81 ε=0.0488 w=0.736 B=2 Sx=0.800
RMS_{dot}=0.02633 RMS_{tot}=0.01331

Appendix. Tone Reproduction Plots

Sample 19: ink= pigmented w/ surf. on top of dyed paper= uncoated
heat= not applied printer= HP1600C

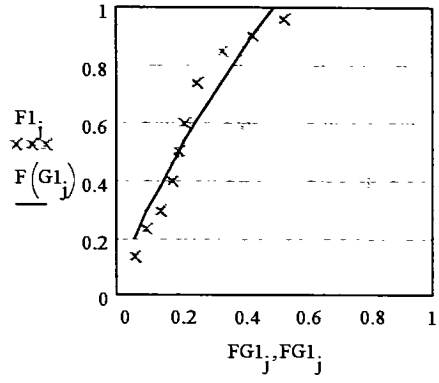

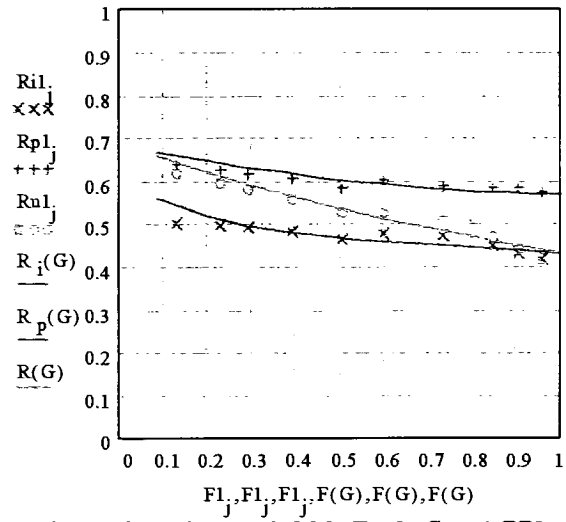

F_r=1.728 m=1.302 c=7.31 R_g=0.68 ε=0.2163 w=0.288 B=2 Sx=4.773
RMS_{dot}=0.07794 RMS_{tot}=0.00946

Sample 20: ink= pigmented w/ surf. on top of dyed paper= synthetic
heat= applied printer= HP1600C

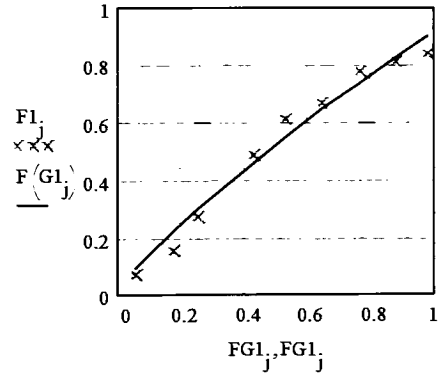

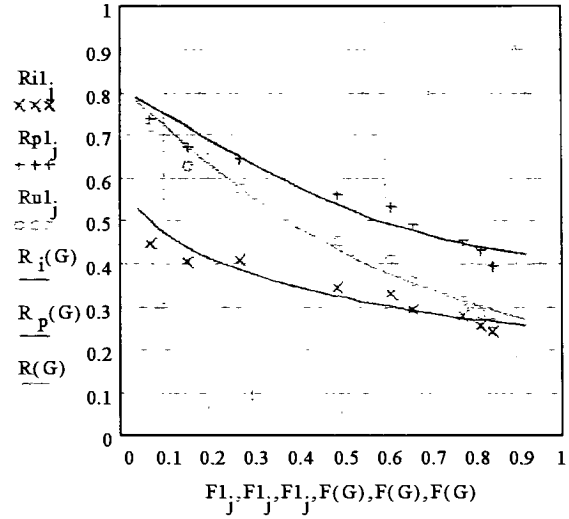

F_r=0.917 m=1.225 c=7.31 R_g=0.81 ε=0.0634 w=0.732 B=2 Sx=0.969
RMS_{dot}=0.04418 RMS_{tot}=0.01662

References

1. J. S. Arney, "A Probability Description of the Yule-Nielson Effect", J. Imag. Sci. & Tech. (1997), in press.

2. J. S. Arney and M. Katsube, "A Probability Description of the Yule-Nielson Effect II: The Impact of Halftone Geometry", J. Imag. Sci. & Tech. submitted (1997).

3. R. Mills, Proc. of 10th Congress on Non-Impact Printing, p. 410 (1994).

4. M. Sklarewitz, IS&T's 47th Annual Conference, p. 823 (1994).

5. R. L. Williams Paper & Ink Relationships Mennonite Press, North Newton, Kansas (1985), p.26.

6. J. S. Arney, C. D. Arney, and M. Katsube, "An MTF Analysis of Papers", J. Imag. Sci. & Technol., **40**: 19 (1996).

7. R. H. Leach, ed., The Printing Ink Manual, 4th ed., Van Nostrand Reinhold (International), London (1988) p.1.

8. R. H. Leach, p. 85.

9. P. Gregory, Proc. of 9th Congress on Non-Impact Printing, p. 275 (1993).

10. R. L. Williams, p. 90.

11. M. Wedin, Modeling of Dot Gain in Halftone Color Prints, Diss. Linkoping University, Linkoping, Sweden (1995) pp.42-44.

12. R. L. Williams, pp. 82-83.

13. J. S. Arney, P. G. Engeldrum, and H. Zeng, "An Expanded Murray-Davies Model of Tone Reproduction in Halftone Imaging", J. Imag. Sci. & Technol., **39**: 502 (1996).

14. J. A. Yule and W. J. Nielson, *TAGA Proceedings*, 1951, p. 65.

15. J. S. Arney, C. D. Arney, and P. G. Engeldrum, "Modeling the Yule-Nielson Halftone Effect," p. 2.

16. F. Ruckdeschel and O. G. Hauser, Applied Optics, **17**, 3376 (1978).

17. M. Wedin and B. Kruse, SPIE Proceedings, Vol. 2413, Color Hard Copy and Graphic Arts IV (1995).

18. B. Kruse and M. Wedin, TAGA proc. p. 329 (1995).

19. S. Gustavson, Proc. of IS&T Conference on Digital Printing, p. 111 (1996).

20. J. C. Dainty and R. Shaw, Image Science, Academic Press, London, p. 258 (1974).

21. J. R. Huntsman, J. Imag. Tech. **13**, 136 (1987).

22. M. Maltz, J. Appl. Photogr. Eng., **9**: 83 (1983).

23. D. R. Watson, Proc. of 9th Congress on Non-Impact Printing, p. 247 (1993).

24. J. C. Dainty and R. Shaw, Image Science, Academic Press, London, P. 258 (1974).